AN ABSTRACT OF THE THESIS OF

Marjorie E. Slauson for the degree of Master of Science in Radiation Health Physics presented on February 8, 2006
Title: Tumor Targeting With a ^{99m}TcMAG-3 Labeled Molecular Engine.

Abstract approved:
Redacted for privacy
Kathryn A. Higley

A unique tumor targeted method, which may be able to deliver a molecule to the surface of a tumor cell using the pH gradient between hypoxic tumor cells and normal tissue has recently been developed. Since solid tumors have been found to have a lower extra cellular pH compared to normal tissue (6.5 to 6.9 for tumors verses an average 7.4 for normal tissue), the pH gradient is used as a source of power to activate a strategically designed "molecular engine" capable of delivering a diagnostic or therapeutic agent to tumor cells. To test this hypothesis, a 22-sequence amino acid, which reorganizes to alpha helical form at pH 6.9 causing the molecule to become lipophilic and embed into the plasma membrane of nearby cells was synthesized. The molecule was then attached to 99mTc via a MAG-3 chelating molecule. *In-vivo* nuclear imaging was performed and showed apparent significant uptake in primary tumors as well as lung and liver in Lewis lung cell model C57blk-J6 mice with confirmed primary tumors at the base of the tail or lungs. This study shows significant promise for early diagnosis and treatment of cancer on a molecular level.

Tumor Targeting With a ^{99m}TcMAG-3 Labeled Molecular Engine

by
Marjorie E. Slauson

A THESIS

submitted to

Oregon State University

in partial fulfillment of
the requirements for the
degree of

Master of Science

Presented February 8, 2006
Commencement June 2006

Master of Science thesis of Marjorie E. Slauson presented on February 8, 2006.

APPROVED Redacted for privacy

Major Professor, representing Radiation Health Physics

Redacted for privacy

Head of the Department of Nuclear Engineering and Radiation Health Physics

Redacted for privacy

Dean of the Graduate School

I understand that my thesis will become part of the permanent collection of Oregon State University libraries. My signature below authorizes release of my thesis to any reader upon request.

Redacted for privacy

Marjorie E. Slauson, Author

ACKNOWLEDGEMENTS

I would like to acknowledge the following people for their support, knowledge and advice. Without their help this thesis would not have been written:

Prof. Kathryn Higley	Major Professor
Prof. John Mata	Co-PI and mentor
Prof. Alena Paulenova	Colleague and mentor
Scott Menn, PhD	Colleague and mentor
Bill Gaeuman	Research Assistant, Statistics
Kevin Dobbs	Student Intern
Natalie Mintz	Veterinary Technician
James Summerton, PhD and staff	Gene Tools, Inc
Prof. Anthony Veltri	Minor Professor
Prof. Barb Watrous	Committee member and mentor
Prof. Steve Binney	Committee member
Prof. Henri Jansen	Graduate Council Representative
Prof. Scott Gustafson	Co-PI

CONTRIBUTION OF AUTHORS

Prof. John Mata assisted with interpretation of chemistry, data collection, data interpretation and writing and editing of sections 1.2, 2.2, 3.1 and 3.2. In addition, Prof. Mata performed the preliminary experimental work outlined in section 1.2.

Bill Gaeuman, OSU statistics department assisted in determining procedures and calculations for uncertainty prediction in all biodistribution calculations.

TABLE OF CONTENTS

Page

1.0 INTRODUCTION 1

1.1. History of Molecular Imaging – the Search for the Magic Bullet 1

1.2 The Molecular Engine 4

1.3 Hypothesis 6

1.4 Study Design 6
1.4.1 Radiolabeling 6
1.4.2 Scintigraphy 7
1.4.3 Health Physics Concerns and Radiation Safety 8

2.0 LITERATURE REVIEW 10

2.1 History of Molecular Imaging 10

2.2 The Molecular Engine 11

2.3 Radiolabeling 12
2.3.1 ^{99m}Tc Carbonyl Complex 12
2.3.2 MAG3 and Other Bi-functional Chelators 13
2.3.3 Quality Control 14

2.4 Scintigraphy 15

2.5 Statistics 15

3.0 MATERIALS AND METHODS 16

3.1. Peptide Labeling 16

3.2. Scintigraphy 17

3.3 Image Analysis and Biodistribution 19

3.4 Biodistribution Using a Gamma Counter 20

3.5 Error Propagation 21

3.6 Health Physics Concerns/Instrumentation 22

3.7 Radiation Safety 23

4.0 RESULTS 25

4.1 Peptide Labeling 25

TABLE OF CONTENTS (CONTINUED)

4.2 Scintigraphy Results 26

4.3 Imaging Biodistribution Results 30

4.4 Gamma Counter Biodistribution Results 34

5.0 DISCUSSION 37

6.0 CONCLUSION 41

BIBLIOGRAPHY 42

LIST OF FIGURES

Figure Page

1.0 Introduction

1.1a) Normal 111-In Labeled Whole Antibody Scan....2

1.1b) Normal 111-In Labelled Antibody Fragment Scan....2

1.1c) Somatostatin Analog....3

1.2a) Action of a Molecular Engine....4

1.2b) Structure of a Molecular Engine in Acidic pH....5

1.2c) Fluorescence Microscopy Results....5

3.0 Materials and Methods

3.1a) MAG-3 chelated to molecularengine....16

3.1b) ^{99m}TcMAG3 Molecular Engine....17

3.3a) Regions of Interest. 20

4.0 Results

4.2.a) Tumors at base of tail visualized by planar gamma scintigraphy.... .26

4.2b) Three Different Treatment Types....27

4.2c) Free ^{99m}Tc vs. ^{99m}TcMAG3peptideimages....28

4.2d) Comparison of Biodistribution for Formula1 verses Formula 2....28

4.2e). Complete image session S3M2....29

4.2f) Complete imaging session of jugular vein injected mouse....29

4.3.a) Percent Injected Dose Lungs....31

4.3b) Percent Injected Dose Liver....32

4.3c) Percent Injected Dose Tumor....33

4.4a) Percent Injected Dose by Gamma Counter....34

4.4b) Comparison of results between gamma counter and gamma camera method....35

LIST OF TABLES

Table Page

1.0 Introduction

1.4a) Mouse Scintigraphy Study Design.....8

3.0 Materials and Methods

3.2a) Mouse Scintigraphy Study Design.....18

3.2b) Injection, Imaging and Analysis Matrix..... 19

4.0 Results

4.3.a) Individual and Weighted Average Percent Injected Dose – Lungs.....30

4.3b) Individual and Weighted Average Percent Injected Dose - Liver.....31

4.3.c) Individual and Weighted Average % Injected Dose – Tumor.....32

4.4a) Gamma Counter Method 24 hr % ID.....34

4.4c) Comparison and % ID for Gamma Camera verses Gamma Counter Results.....36

LIST OF APPENDICES

Appendix — Page

A) Raw Images

A.1) Imaging Session 1 46

A.2) Imaging Session 2 47

A.2) Imaging Session 2 48

A.3) Imaging Session 3 49

A.4) Imaging Session 4) 50

B) Raw Data

B.1) Imaging Session 1 51

B.2) Imaging Session 2 52

B.3) Imaging Session 3 53

B.4) Imaging Session 4 54

C) Calculations

C.1) Calculations for Percent Injected Dose Gamma Camera and Error Propagation 55
(a) Injected Dose Organ 55
(b) Error Propogation 55

C.2) Calculations for Injected Dose Gamma Counter (24 hr) and Error Propagation 56
(a) Data 56
(b) Gamma Counter Efficiency 56
(c) Percent Injected Dose 56
(d) Error Propagation (Gamma Counter Method) 57
(e) Error Propagation (Gamma Counter Method) continued 58

C.3) Weighted Averages 58

Appendix D – Calibration and Efficiency of Gamma Camera

D.1 Materials and Methods 59

D.1.2 Photo Peaking 59
D.1.3 Energy Resolution 59
D.1.4 Flood Field Uniformity 60

D.2 Gamma Camera Efficiency 60
D.2.1 Materials and Methods 60
D.2.2 Gamma Camera Results 62
D.2.3 Conclusion 63

LIST OF APPENDICES (CONTINUED)

Appendix E – Calibration of Dose Calibrator

E.1 Materials and Methods 64
E.1.1 Accuracy 64
E.1.2 Geometric Dependence 64
E.1.3 Linearity 64
E.1.4 Correction Factor for Accuracy 65

E.2 Results 65
E.2.1 Accuracy 65
E.2.2 Geometric Dependence 66
E.2.3 Linearity 67
E.2.4 Correction factor for Accuracy 68

E.3 Conclusion 68

F.1 Materials and Methods 72

F.2 Results 73

F.3 Conclusion 73

LIST OF APPENDIX FIGURES

Figure Page

A) Raw Images

A.1a) Image Session 1 46

A.2a) Image Session 2 Free ^{99m}Tc Tumor and Non-tumor controls 47

A.2b) Image Session 2 48

A3a) Image Session 3 49

A.4a) Image Session 4 50

D) Calibration and Efficiency of Gamma Camera

D.2a) Gamma Camera Efficiency 61

E) Calibration of Dose Calibrator

E.2.3b) Linearity for Victoreen Cal/Rad 67

F) Dose Estimation to Extremities for Imaging

F.1a) Input parameters for MicroShield code 72

LIST OF APPENDIX TABLES

Table		Page
B)	Raw Data	
B.1a)	Raw Data for 1st Imaging Session	51
B.2a)	Raw Data for 2nd Imaging Session	52
B.3a)	Raw Data for 3rd Imaging Session	53
B.4a)	Raw Data for 4th Imaging Session	54
D)	Calibration and Efficiency of Gamma Camera	
D.2b)	Gamma Camera Efficiency	62
D.2c)	Calculated Efficiency, SD and Chi Sq for gamma camera	63
E)	Calibration of Dose Calibrator	
E.2a)	Dose Calibrator Accuracy Check	66
E.2b)	Geometry Data for Victoreen Dose Calibrator	66
E.2.3a)	Data for Victoreen Cal/Rad Dose Calibrator linearity determination	67
E.2.4a)	Data for accuracy correction factor of Cal/Rad Dose Calibrator	70
E.2.4b)	Data for accuracy correction factor of Cal/Rad Dose Calibrator	71
F)	Dose Estimation to Extremities for Imaging	
F.2a)	Calculated total dose to extremities per imaging session	72

1.0 Introduction

1.1. History of Molecular Imaging – the Search for the Magic Bullet

Over the last 20 years monoclonal antibodies (MoAbs) have been studied and employed as a means for diagnosing and treating different types of cancer. Monoclonal antibodies are similar in structure and biological action to natural antibodies and are produced in response to foreign substances in the body (antigens). This unique tumor targeted method, based on tissue function rather than anatomy, employs a radioactive tracer or therapeutic agent attached to a cloned antibody to target antigens specific to tumor cells. Generally, the method of action for MoAbs is to attach to a specific receptor site on the surface of a tumor cell and deliver a cytotoxic or radiolabeled molecule. Early attempts at using whole antibodies for diagnostics or therapy suffered from human immune response reactions due to the common production of MoAbs from mouse cells and delayed excretion from vital organs such as the liver and kidneys. In addition, the large size of MoAbs keeps the smaller functional molecule from reaching many tumor cells. (Fiola, 2003) Attempts to reduce the size and toxicity of MoAbs have resulted in production of MoAbs that are cloned from human or hybrids of human and mouse cells to reduce systemic immune reaction and smaller antibodies such as diabodies and fragments that retain specificity and have faster clearance times from vital organs. Advances in production and application of MoAbs have resulted in several FDA approved diagnostic and therapeutic radiopharmaceuticals since the early 1990's (Henkin, 2001) *(figures 1.1a and 1.1b).*

In the past decade, the integration of expertise from cellular biology, molecular biology and diagnostic imaging has given rise to an emerging new field termed "molecular imaging". The basic principle of this application is for molecular biologists to characterize the disease to be studied on the molecular level and design and label agents to bind specifically to identified target molecules. (Rollo, 2003). These agents have the common term "molecular probe". Molecular imaging follows logically from the first attempts at diagnosis and therapy with monoclonal

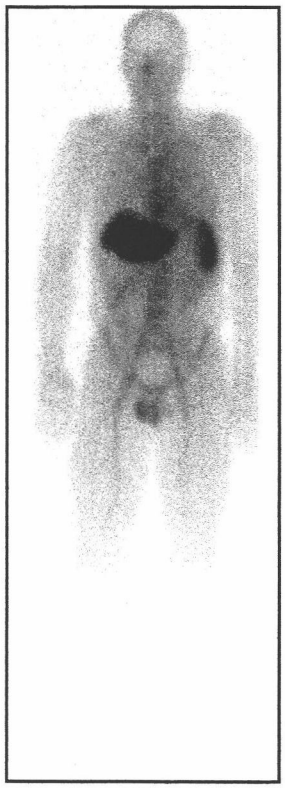

Figure 1.1a

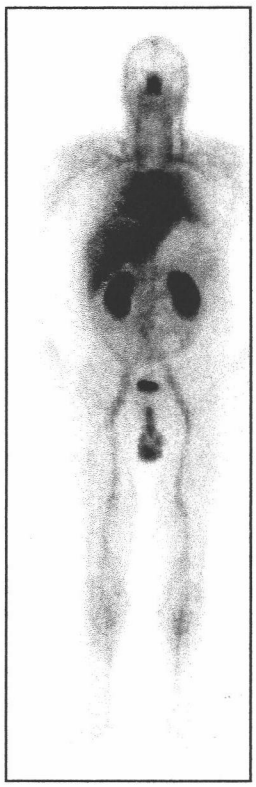

Figure 1.1b

Figure 1.1a) Normal ^{111}In labeled whole antibody scan (OncoScint) at 4 days post injection. Note the delayed excretion from the liver and spleen. (Kansas University Medical Center, Nuclear Medicine teaching Files, 2005)

Figure 1.1b) A normal antibody fragment (CEA scan) scan at 4 hours post injection. Note increased uptake in liver and kidneys. Both of these MoAbs are now in clinical use for in-vivo detection of tumors. (Kansas University Medical Center, Nuclear Medicine teaching Files, 2005)

antibodies and fragments. An example of molecular imaging is the use of the specific binding of peptides to their receptors to selectively target a specific tumor type and visualize cellular processes *in-vivo*. Advantages of this technology are much smaller, molecular sized delivery agents, which theoretically should show more specific localization at the tumor and produce faster pharmacokintetics. In addition, because of the molecule's smaller size there is a potential for the peptide to cross the cellular membrane for intracellular

delivery of a cytotoxin. One of the first successful applications of molecular receptor imaging in nuclear medicine came in the early 1990's with the production of a somatostatin analog. The somatostatin receptor peptide attaches to the somatostatin receptor expressed by neuroendocrine and a number of other tumor types *(figure 1.1c)*. Being of a size much closer to cellular level, the main route of excretion for the somatostatin receptor analog and other peptides is the kidneys, rather than the liver, and these smaller molecules are typically cleared from the blood more rapidly than MoAbs and fragments. (Langer and Beck-Sickinger, 2001).

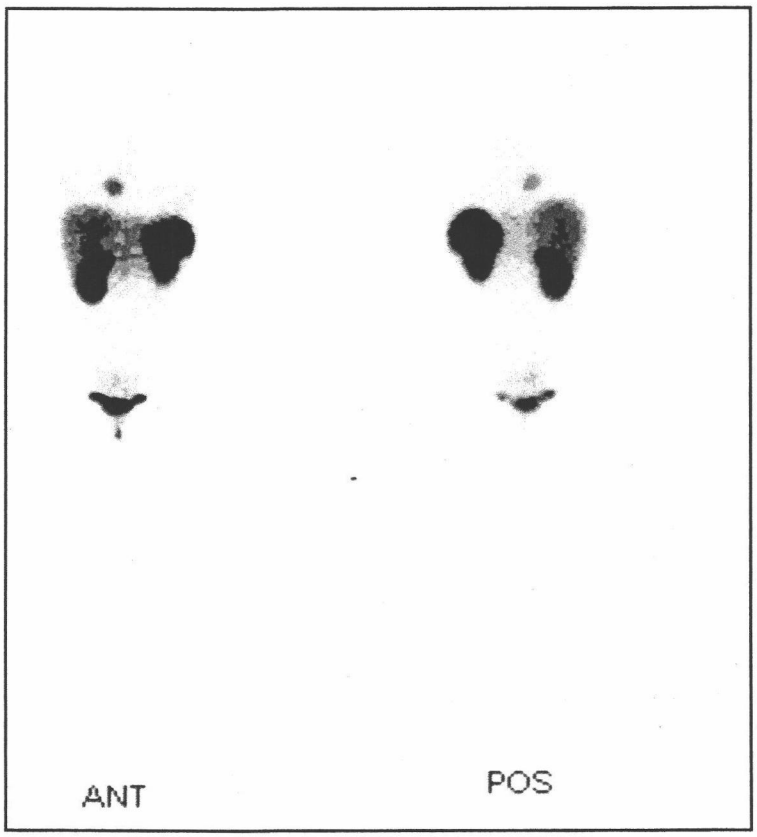

Figure 1.1c) Somatostatin Analog (^{111}In-Pentreotide) 48 hours post injection. Note delayed excretion from the kidneys, increased plasma (background) clearance over whole antibodies and fragments and abnormal focal area above the liver (Pheochromocytoma). (Cottin et.al, 1999)

With the emergence of the field of molecular imaging the potential for development of novel imaging and therapeutic agents on the molecular level that

can be translated to *in-vivo* human use is increasing. The molecular "magic bullet" will successfully target a variety of tumor types in concentrations high enough for diagnosis and therapy while eliminating rapidly from the bloodstream and non-target organs.

1.2 The Molecular Engine

Solid tumors have a lower than normal extracellular pH (Wilke-Hooley et. al., 1985). In 1997 a first generation "molecular engine" capable of transporting a molecule across the endosomal membrane to the cytosol of a tumor cell using the pH gradient between normal tissue and hypoxic tumor cells as a source of power was developed (Summerton and Weller, 1997). The molecular engine differs from previously developed molecular probes in that it does not rely on identifying a binding site on the surface of the targeted cell and it displays a steep transition from its water soluble random coil confirmation lipophilic conformation. This more passive mode of action makes the molecular engine attractive for any tumor cell that exhibits a markedly different pH than normal tissue. At high pH the peptide engine exists in a water soluble, relaxed coil and upon acidification at the designed pH of activation, the peptide undergoes transition to its lipid-soluble, α-helical form, allowing the endosomal membrane to draw the molecule into the cytosol of the cell. *(figure 1.2a)*

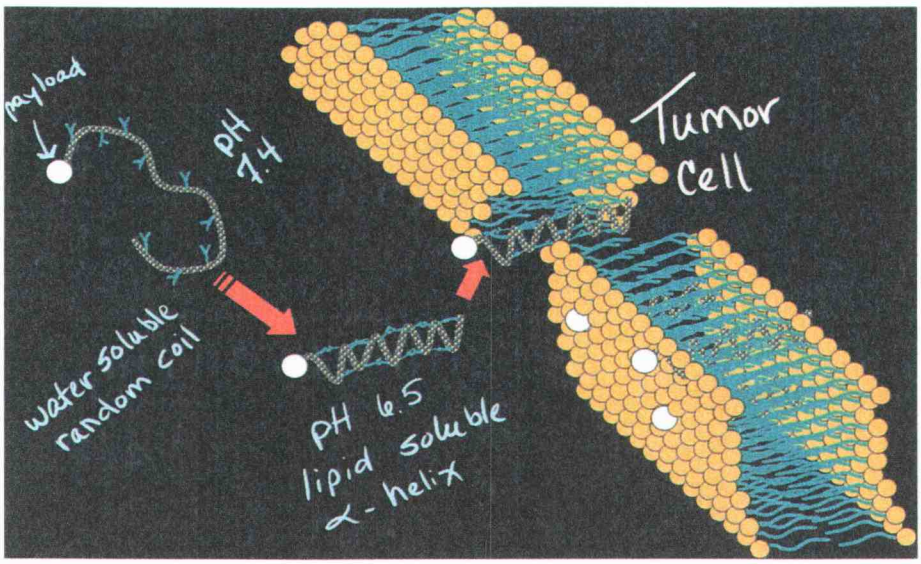

Figure 1.2a) Action of a molecular engine.

Within the cytosol where the pH is once again high, the molecule relaxes, delivering its payload of radiotracer, cytotoxin, or custom therapeutic. Through changes in the peptide sequence and composition, the pH of activation can be engineered to accommodate a desired target pH. The basic structure of the molecular engine at acidic pH is shown in figure 1.2b.

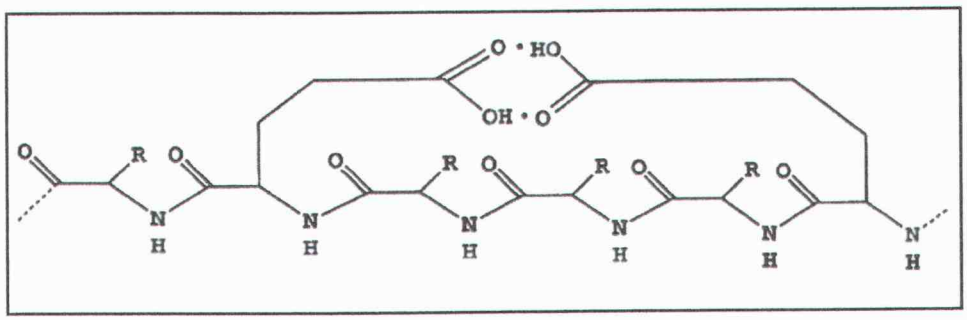

Figure 1.2b) Structure of a molecular engine in acidic pH.

Studies using a 22 amino acid peptide designed for activation at pH of approximately 6.9 and labeled with a fluorescein molecule (FITC) demonstrated the molecular engine was capable of concentrating at tumor cells (Mata et al., 2005). The FITC labeled molecule was delivered *in-vivo* to mice bearing Lewis lung cell derived tumors. Fluorescence microscopy showed increased accumulation of the FITC labeled peptide at the tumor site (*figure 1.2c).*

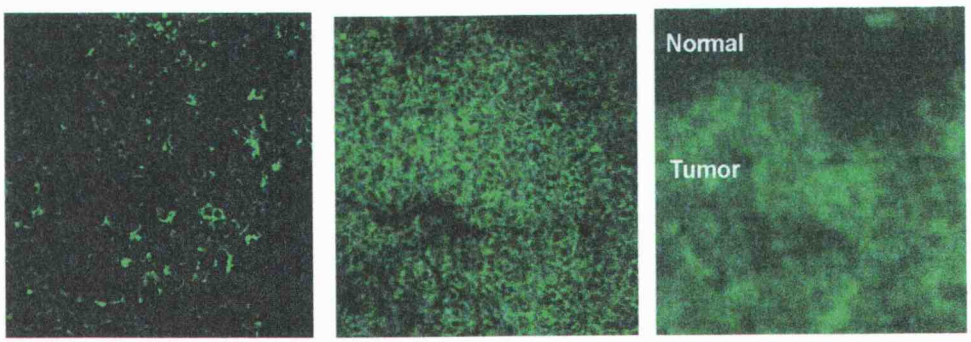

Figure 1.2c) Fluorescence Microscopy Results. Mice were treated with saline only and FITC labeled peptide. Tumors were excised and tissue analyzed with fluorescence microscopy. The image at the left shows saline-only (background) treated tissue. The middle image shows FITC labeled peptide treated tissue and the image at the right shows the demarcation between normal and tumor in FITC labeled peptide treated tissue.

1.3 Hypothesis

Using a rationally designed molecular engine capable of forming an alpha helix at pH 6.9 it will be possible to label the molecular engine peptide with a radioactive tracer via a complimentary ligand and visualize accumulation within tumors *in-vivo*.

1.4 Study Design

The identification of possible ligands for radioactive tracer attachment to the molecular engine, labeling the chelated peptide, and *in-vivo* imaging of tumors with the radiopharmaceutical to determine overall efficacy and biodistribution of the peptide in mice were the main goals of my work on this project. Radiation Safety and instrumentation calibration methods for this experiment are also included in the appendices to this publication.

The disease model was lung cancer using C57blk-J6 mice injected with Lewis lung cancer cells at the base of the tail.

1.4.1 Radiolabeling

^{99m}Tc was identified as the initial radioactive tracer of choice over ^{111}In or ^{131}I because it is commonly used in nuclear medicine diagnostic studies, has a very short half-life, has desirable characteristics for labeling, and the monoenergenic, 140 keV gamma emissions produce favorable gamma imaging characteristics. In addition, radiometals such as ^{99m}Tc or ^{111}In labeled moabs and peptides have a longer retention period in tumors than iodinated proteins (Anderson, 2001).

Requirements for the ligand used to attach the molecular engine to ^{99m}Tc were that it must not change the action of the peptide, it should be relatively small in size and molecular weight compared to the peptide, and that it would provide high yields of the desired imaging agent. An extensive literature review produced two likely chelating agents that could be attached during production of the molecular engine peptide. The first, a ^{99m}Tc carbonyl complex, was discarded after repeated attempts by

Gene Tools, Inc. failed to attach the histidine chelator complex to the 'N' terminus of the molecular engine peptide. Mercaptoacetyltriglycine (MAG3) was then chosen as the ligand due to more favorable peptide labeling conditions. The MAG3 was attached during production of the molecular engine peptide at Gene Tools, Inc. and the MAG-3 conjugated peptide (MAG3 ME) was delivered to the lab ready for labeling with ^{99m}Tc.

Labeling and bench top quality control of the MAG3 ME with ^{99m}Tc was derived from a previously published process (Rusckowski et. al, 2001) with minor modifications.

Two generations of ^{99m}TcMAG3 ME (Gen1 and Gen2) have been studied to date. The Gen1 was the initial 22 amino acid molecular engine peptide (Mata, 2005) designed to activate at a pH of around 6.9. Gen2 was developed 1 month into the imaging phase of the study and was designed to activate at a pH closer to 7.0. The Gen2 ^{99m}TcMAG3 ME mice are not considered in this publication.

1.4.2 Scintigraphy

Initially, the imaging phase of the study was to involve 250 mice treated with different iterations of the molecular engine peptide and sacrificed at incremental times post injection to determine pharmaceutical kinetics. With this model, 6 mice for each time point could be imaged at once and a potential of 30 mice per imaging session could be realized, with 5 time points post injection. Over the course of the planning phase, however, it was determined that the mice should be anesthetized and imaged at incremental time points over the entire course of the imaging session, since this model would more closely imitate a clinical treatment. This approach necessitated a decrease in the number of mice involved in the study and was viewed by the research group as a more humane treatment overall. The final number of mice used for this thesis was 20, with

research by the group ongoing. Table 1.4a shows the final study design for this publication.

Table 1.4a) Mouse Scintigraphy Study Design. Numbers in the boxes indicate number of animals per treatment type.

	LLC Model (# of Mice)	No Tumor (# of Mice)
Free 99mTc ($NaTC0_4$-)	2	2
99mTc-MAG3-ME	12	3
99mTc-MAG3-ME Jugular Vein Injection (JI)	1	0

S

Static imaging was performed on an IS2 Medical Systems rectangular, single head gamma camera fitted with a high resolution, low energy collimator. The timed image points were at 1, 2, 4, 8 and 24 hours post injection of 37 MBq (1 mCi) of 99mTcMAG3 ME.

1.4.3 Health Physics Concerns and Radiation Safety

During the design and experiment phases of the study health physics instrumentation needs were identified which included the gamma camera, personal dosimeters (both TLD and immediate read ionization chambers), a dose calibrator to determine injected dose and quality control parameters, a gamma counter for quantification of organ uptake, suitable shielding and various survey instrumentation such as pancake G-M and dose rate survey instruments. In addition a separate laboratory for radiolabeling was required which necessitated the movement of radioactive materials and some of the instruments from one place to another.

Adequate shielding during labeling, potential excessive exposure to extremities during injection and imaging, processing of radioactive animals, tissue samples, and waste, and proper packaging and shielding

during transportation were revealed as areas of concern in the safety review performed during the design phase of the study.

While most of the required counting equipment was available, proper calibration was questionable for the gamma camera and dose calibrator. Therefore, calibration of these instruments was performed prior to any experiments being carried out. Calibration of the gamma camera and dose calibrator are treated as supporting experimental data. (Appendix D and E).

Since no shielding would be used during anesthesia and imaging of the radioactive mice, the dose to the extremities of the primary animal handlers was identified as an area of concern. A dose estimate was performed prior to the study using MicroShield version 5.5 for the extremities during anesthesia and imaging. (Appendix F).

2.0 Literature Review

2.1 History of Molecular Imaging

In 2003, Catherine Fiola summarized the development of monoclonal antibodies as anticancer agents. In the 1950's, Pressman and Goldman discovered that antibodies could specifically target tumor cells. In 1975 a technique for creating monoclonal antibodies was demonstrated by Kohler and Milstein. Over the last three decades monoclonal antibodies and antibody fragments have been developed to selectively diagnose and treat cancer.

As Henkin wrote in his 2001 article regarding the growing use of antibodies and peptides in clinical nuclear medicine, and as found at the Radiopharmacy, Inc.website (http://www.radiopharmacy.com/product.shtml) there are now many FDA approved antibodies and peptides in use for selective diagnosis of a number of cancers. These include OncoScint® CR/OV (^{111}In Satumomab Pendetide) for imaging of metastatic disease from colorectal or ovarian cancer, CEA Scan® (^{99m}TC Acritumomab) for imaging of colorectal cancer, and Octreoscan® (^{111}In Pentetreotide) a somatostatin analog for imaging of neuroendocrine tumors.

As Fiola also mentioned, many obstacles in the development of monoclonal antibodies have been encountered such as human immune response to murine mouse antibodies, prolonged localization in non-target tissues such as the liver and kidneys, and complications to specificity due to the large size of monoclonal antibodies.

In his 2003 article, Rollo described molecular imaging as a "new discipline in medicine which has evolved over the last decade". The basis of this application is the "identification of specific receptor sites associated with target molecules that characterize the disease process to be studied". Molecular imaging agents are then created to bind specifically to the target molecules of interest and, in nuclear medicine, are labeled with a radioactive substance to create a "molecular probe" capable of determining the location of all targeted molecules within the body when imaged.

Commonly found in the literature regarding receptor imaging (Rollo, Langer-Sikinger, Gilles and Fiola), the first successful and FDA approved molecular probe was the somatostatin analog which binds to somatostatin receptor sites on neuroendocrine tumors. This initial success opened the floodgates of research into molecular imaging agents.

2.2 The Molecular Engine

Not quite analogous to the "molecular probe", although its method of action is also on a cellular level, is the "molecular engine" which was developed by Summerton and Weller in 1997.

In 1985, Wike-Hooley et al., published a paper which established that human tumor pH was significantly lower then normal blood or tissue pH. This is the basis for the development of the molecular engine.

In their 1997 paper, Summerton and Weller described the action of the molecular engine which changes shape to alpha-helical form upon entering a lower than normal pH environment such as a cellular membrane during the late endosome or early lysosome stage following endocytosis of macromolecules. The development of molecules capable of activation at pHs in the higher pH range of 6.7-7.0 allowed Summerton and colleagues to envision targeting areas of low pH found in disease states including the extracellular environment found in tumors. The pH gradient within tumors would provide the source of energy to power the delivery of a small peptide. A properly designed molecular engine should be able to embed onto the membrane during low pH conditions, or could be modified to pull an attached cytotoxin into the cytosol of the cell.

In 2005, Mata et al. demonstrated that a peptide based probe was capable of changing shape at pH of 6.9 (approximating tumor pH) and embedding into the plasma membrane of tumor cells.

2.3 Radiolabeling

2.3.1 ^{99m}Tc Carbonyl Complex

In 1998, Alberto, Schibli, et al. introduced the "first synthesis of a water and air stable organometallic aqua complex [$^{99m}Tc(OH_2)_3(CO)_3$]", also called ^{99m}Tc(I)-carbonyl complex. The substitution of the water ligands by a bifunctional ligand would enable a simplified attachment to a biomolecule under aqueous conditions. This was the first instance published of direct labeling of the common $^{99m}TcO_4^-$ entity without the necessary reduction step required to attain a +5 valence. In addition the labeling process was straightforward, the bifunctional ligand could be any amino acid attached to the biomolecule of interest, and would likely not interfere with the action of the peptide.

In 1999 Weibel et al. reported a stable histidine tagged protein labeled with the ^{99m}Tc(I)-carbonyl complex under STP conditions, which resulted in yields greater than 95%. Biodistribution in mice was favorable for rapid blood clearance of this particular protein. Significantly, these yields were higher than in other reported studies of 99mTc(I)-carbonyl complex and it was thought that the 'N' terminus of the histidine played a significant role in the high label yields and stability of the molecule.

In 2004 Schirmacher et. al, described labeling an L-tyrosine derivative with the ^{99m}Tc(I)-carbonyl complex using a kit for the procedure developed by Mallinckrodt called Isolink®. Again, high yields for the radiolabeled biomolecule were reported. A benchtop quality control method using radio-HPLC was also described in this paper.

The advent of the kit and acquired instructions from Mallinckrodt broke the process down into one step for radiolabeling once a suitable histidine "bridge" was attached to the 'N' terminus of the molecular engine. Unfortunately, however, the attachment of the ligand to the 'N' terminus of the molecular engine was complicated by the need to protect the double

bonded oxygens in order to retain the action of the orginal molecular engine. This ligand was scrapped after repeated attempts to attach it.

2.3.2 MAG3 and Other Bi-functional Chelators

More extensive literature review yielded other likely chelators such as Ethylene-dicysteine (EC), which is being developed in the United States as a ^{99m}Tc renal imaging agent with favorable plasma and renal clearance over ^{99m}TcMAG3 (Verbruggen at al., 1991 and Taylor et al., 1997) In addition, EC has been used as a ligand to radiolabel endostatin by Yang et al. in 2002 and Annexin V (Yang et al., 2001) It was shown that ^{99m}Tc-EC-Endostatin does not alter the *in-vivo* behavior of endostatin and ^{99m}Tc-EC-Annexin V showed increased uptake in irradiated breast cancer cells in rats. Gamma camera planar imaging showed favorable results for tumor visualization for both ^{99m}Tc-EC-Endostatin and ^{99m}Tc-EC-Annexin V. EC may be used in the future as a ligand for labeling the molecular engine.

Diethylene-triamine-pentacetate (DTPA), also a ^{99m}Tc renal imaging agent was considered early on in the planning phase, but was dropped in favor of Mercapto-acetyl-triglycine (MAG3). According to Zhang, Liu, et al. in their 2000-2002 investigation of different chelators and biodistribution in mice of ^{99m}Tc-Morpholinos, MAG3 exhibited faster plasma and renal clearance, in addition for tumor bearing mice, the ^{99m}Tc-Morpholinos were cleared more rapidly from the kidneys and whole body while a high concentration was found in tumor at 24 hours according to biodistribution results. Images reflected high uptake in tumors and low uptake in the rest of the body of the mice.

The 1998 publication by Hnatowich et al. describes using MAG3 as a bifunctional chelator for ^{99m}Tc labeling of an array of small peptides and the 2001 paper by Ruskcowski et al. described a peptide labeled with ^{99m}Tc by 4 different methods using an array of chelators. From these publications, MAG3 was determined to be the best choice of bifunctional

chelator for this experiment. A labeling method and quality control using benchtop radio-HPLC was also described in both the Hnatowich and Ruskowski papers, which was slightly modified for the molecular engine.

2.3.3 Quality Control

A quick and easy method for rapid determination of labeling efficiency using benchtop solid phase extraction was described in the 2001 publication by Rusckowski et al.. This method separates unbound ^{99m}Tc and small ionic impurities from the bound protein. While this procedure was employed for our labeling and provides a quick analytic method for determination of labeled fractions, a more rigorous quality control should be employed for absolute quantification of labeling efficiency which excludes isomers of the original peptide and other labeled protein impurities by size.

A coordinated research project funded by the International Atomic Energy Agency (IAEA) in 1995-1999 entitled "^{99m}Tc labeled peptides for imaging of peripheral receptors", April 2001, describes a number of labeling procedures, high purity liquid chromatography (HPLC) and other analytical techniques for labeled peptides. From this report, a number of HPLC solid phase and solvents for liquid phase were identified; however, none seemed appropriate for our molecular engine In addition, the report reiterated that while benchtop quality control methods were acceptable, they should be used in conjunction with HPLC to quantify insoluble components.

The Grace Vydec "Handbook of Analysis and Purification of Peptides and Proteins by Reversed Phase HPLC" describes in-depth the theory and methods for reverse phase HPLC. From this handbook, it was determined that a likely method to try for our molecular engine would be to use a C-18 reverse phase column with acetonitrile or tri-flouro acetic acid in a gradient elution for the mobile phase.

2.4 Scintigraphy

Procedures for calibration, tuning and general imaging protocols for the IS2 gamma camera were found in the procedure manual (IS2 Medical Systems, 2004) In the 2003 publication entitled "Can Tumor Uptake Tc-99m MDP?", Fang described mouse dosing, imaging and biodistribution analysis protocols. Mice were injected with 74 MBq (2 mCi) in 0.05 ml MDP solution after allowing implanted tumors to reach approximately 1 cm in diameter (4-5 weeks). Planar imaging was performed in a 512 x 512 x 16 pixel matrix to 500 – 800K counts at 6 hours post injection. Biodistribution analysis compared cpm/pixel within the tumor region of interest to cpm/pixel within a spine region of interest to determine the tumor positive value over the target organ (bone) for MDP. Parameters from Fang's study were modified to fit this experiment.

2.5 Statistics

Statistics for analyzing error in the biodistribution results were taken from a number of sources. A process for determining error for a single determination when adding or multiplying counts is described by Knoll (1975) in the first edition of his publication entitled "Radiation Detection and Measurement". A more thorough description of this method as derived from a Taylor expansion formula was found in the "Measurement Process Characterization Handbook" on the National Institute of Standards (NIST) website at www.nist.gov and summarized by Wittke in 2003 at http://jan.ucc.nau.edu/~wittke/Microprobe/Statistics-Error.html. A discussion and application of weighted averages and error for the calculation was found in Wang, et al., (1975) Radiotracer Methodology in the Biological, Environmental, and Physical Sciences.

3.0 Materials and Methods

3.1. Peptide Labeling

The molecular engine peptide was conjugated to mercaptoacetyltrigylcine (MAG3) at Gene Tools, Inc. and delivered to OSU Veterinary Medicine ready for radiolabeling with ^{99m}Tc. (Figure 3.1a)

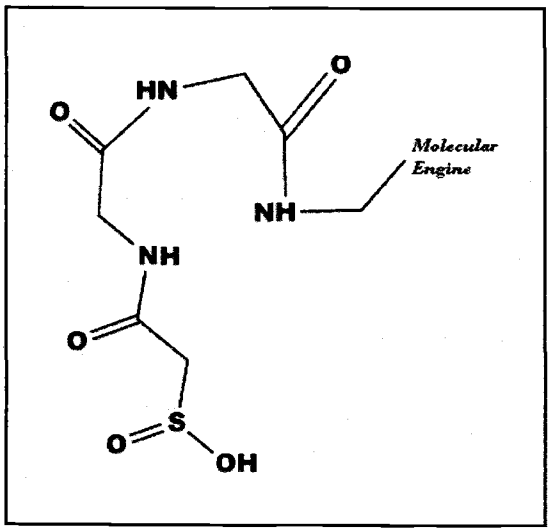

Figure 3.1a) MAG-3 chelated to molecular engine. .MAG3 was chelated to the molecular engine at Gene Tools, Inc. and delivered to the lab ready for radiolabeling with ^{99m}Tc.

For ^{99m}Tc labeling, the conjugated peptide was diluted to 4.0 mg/ml in 250 µl 5% sodium bicarbonate in normal saline, pH approximately 7.0. A labeling solution was prepared according to a procedure outlined by Rusckowski et. al., (2001) with minor modifications as follows: First a tartrate solution was prepared by adding 2.1 g Sodium Bicarbonate, 0.96g Ammonium Acetate and 0.31 g Ammonium Hydroxide to a solution of 50.0 mg/ml Sodium Tartrate. Labeling was then performed by adding 30 µl of the tartrate solution to the peptide reaction vial containing 1.0 mg of peptide, followed by 740 MBq (20 mCi) $Na^{99m}Tc0_4$-. Finally, 10 µl of 1 mg/ml $SnCl_2$, prepared with 10 mmol HCL was added to reduce the valence of the 99mTc pertechnetate to +5 and the solution was incubated at room temperature for 30 minutes. (figure 3.1b)

The final specific activity of the labeled peptide was approximately 740 MBq/ml (20 mCi/ml) for a final injection volume of 50 µl (Formula 1). For the 3rd and 4th

labeling procedures, 250 µl 5% injectable mannitol was added to the final labeled peptide solution in order to reduce the effect of peptide aggregation (Formula 2).

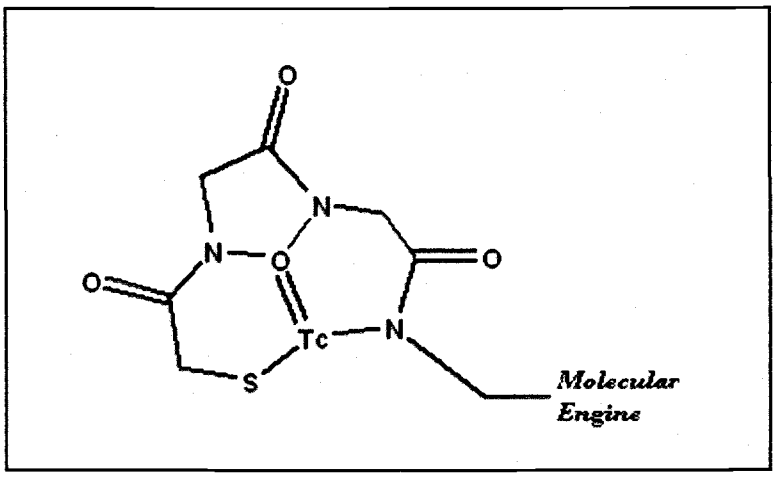

Figure 3.1b) ^{99m}TcMAG3 Molecular Engine.

Labeling efficiency was determined using reverse phase bench top liquid chromatography as follows: A Sep Pak C18 mini cartridge was prepared by flushing with 10.0 ml ethanol, followed by 10.0 ml sterile H_20 and finally, purged with 5.0 ml air. Approximately 100 µl of labeled peptide was loaded onto the cartridge, which was then eluted with 5.0 ml 1.0 mmol HCl to remove any free $99mTc0_4$- and 99mTc-tartrate, followed by 5-10 ml 5% $NaHC0_3$ to recover the labeled peptide. The elution fractions were then assayed on the Victoreen Cal/Rad dose calibrator and labeling efficiency was calculated based on the assay measurements. Radiolabeling efficiency was equal to the assayed dose in the peptide solution divided by the assayed dose in the peptide solution plus the assayed dose in the free ^{99m}Tc/^{99m}Tc-Tartrate solution. Doses of approximately 37 MBq (1 mCi) ^{99m}Tc-MAG3 labeled molecular engine (^{99m}Tc-MAG3 ME) were drawn for each animal.

3.2. Scintigraphy

Four imaging sessions were performed over a period of four months. A total of 15 mice were injected with 50,000 Lewis lung cancer cells (LLC1) via the tail vein 2-4 weeks prior to the study. Of the 15 mice injected with LLC1 cells, 2 were used as free ^{99m}Tc controls, 12 were injected with the ^{99m}TcMAG3 ME via

the tail vein and 1 was injected with ^{99m}TcMAG3 ME via a cut down followed by direct injection to the jugular vein (JI). In addition 5 tumor free control mice were injected: 2 mice were injected with free ^{99m}Tc and 3 mice were injected with ^{99m}TcMAG3 ME. The total number of mice in this study was 20. 9 LLC1 mice were injected with Formula 1, 4 LLC1 mice and the LLC1 JI mouse were injected Formula 2 ^{99m}TcMAG3 ME (mannitol added to final labeling solution). Table 3.2a shows the matrix for the study design.

Table 3.2a) Mouse Scintigraphy Study Design. The numbers in the boxes indicate number of animals per treatment type.

	LLC Model (# of mice)	No Tumor (Control) (# of Mice)
Free ^{99m}Tc ($NaTC0_4$-) Formula 1	2	2
^{99m}Tc-MAG3 ME Formula 1	7	2
^{99m}Tc-MAG3 ME Formula 2	5	1
^{99m}Tc-MAG3 ME JI Formula 2	1	0

Mice were anesthetized and injected with 25.9 to 37.0 MBq (0.7 to 1.0 mCi) ^{99m}TcMAG3 ME or 25.9 to 37.0 MBq (0.7 to 1.0 mCi) 99mTc sodium pertechnetate via the tail vein. Mice were anesthetized during each procedure and were awake with access to food and water *ad libitum* between imaging sessions. Positioning was AP to the face of the gamma camera at a distance of 5 cm. All images were acquired on the IS2® single head gamma camera fitted with a low energy, high resolution collimator, peaked at 141 keV for ^{99m}Tc with a 20% window in a 512 x 512 x16 pixel matrix. Static images were performed at 0, 2, 4, 8, and 24 hours post injection. Aquisition time ranged from 2 to 20 minutes depending on time between injection and imaging. Mice were imaged to an end point of 8 hours in imaging session 1 and an endpoint of 24 hours in imaging

sessions 2, 3 and 4. Imaging endpoint is the time mice were euthanized, except for imaging session 3. In imaging session 3 one tumor positive mouse died prematurely and was imaged to an endpoint of 8 hours and another tumor positive ME mouse died prematurely at 4 hours and was not included in the analysis. (Table 3.2b) Table 3.2b shows the final matrix for imaging and analysis. Images were collected at previously mentioned time points up until the imaging endpoint.

Table 3.2b) Injection, Imaging and Analysis Matrix. This table shows number of mice per treatment type, imaging end point, and analysis methods.

Imaging Session	Radio-Pharmaceutical	Number of LLC1 Mice Imaged	Number of "no-tumor" Control Mice Imaged	Imaging End Point (hours post injection)	Image Analysis/ Biodistribution Methods
1	^{99m}TcMAG3 ME Formula 1	3		8	Camera ROI, Visual
2	^{99m}TcMAG3 ME Formula 1	4	2	24	Camera ROI, Visual
	Free ^{99m}Tc	2	2	8	Visual
3	^{99m}TcMAG3 ME Formula 2	3[1]	1	24	Gamma counter, Camera ROI, Visual
4	^{99m}TcMAG3 ME Formula 2	2		24	Camera ROI Visual
	^{99m}TcMAG3 ME (JI) Formula 2	1		24	Camera ROI Visual

[1] One mouse in this session died prematurely and was imaged to an endpoint of 8 hours and one died at 4 hours and was excluded from analysis.

3.3 Image Analysis and Biodistribution

Biodistribution curves were generated for the ^{99m}TcMAG3 ME mice that had an imaging end point of 8 hours or greater. Free ^{99m}Tc control images from all sessions were analyzed visually only.

Viewing and analysis of static images was performed on a Hermes Gold ™ workstation. All images were analyzed visually for biodistribution. 12 mice injected with Lewis Lung cells and ^{99m}TcMAG3 ME and 1 ^{99m}TcMAG3 ME

control were analyzed for *in-vivo* pharmacokinetics using the Hermes Gold workstation. Injected dose was determined by using the Hermes software to draw a region of interest (ROI) around the entire mouse for T=0 images and a background region in the soft tissue away from obvious areas of uptake in the body of the mouse. Regions of interest were also drawn for all images at each time point around lungs and liver[1], tumor, and a background region drawn in the abdomen adjacent to the kidneys. (figure 3.3a) Results for each organ and whole body were background subtracted using CPM/pixel for the region and then normalized to number of pixels per organ. CPM/organ was then compared to CPM/whole body at T=0 to obtain percent injected dose in the organ (% ID). This result was then decay corrected for all time points to the injection time (T_0) to graphically visualize the pharmacokinetics of the molecular engine disregarding radioactive decay.

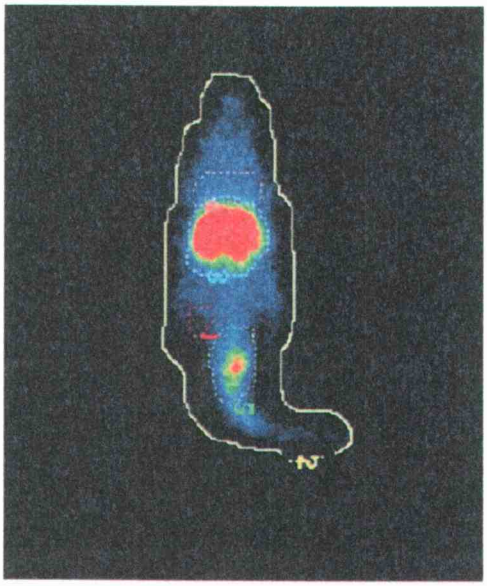

Figure 3.3a) Regions of Interest. Regions of interest were drawn over organs where uptake was readily visualized. CPM/pixel was collected for each region in each image to obtain biodistribution curves.

3.4 Biodistribution Using a Gamma Counter

From imaging session 3 the ^{99m}TcMAG3 ME tumor free control mouse and an LLC1 ^{99m}TcMAG3 ME mouse were sacrificed immediately after the 24 hour

[1] Liver was visualized in studies 3 and 4 only.

imaging time point and biodistribution curves were generated using the gamma counter.

One mouse positive for tumor at the base of the tail and one control mouse (no tumor) were analyzed for ^{99m}TcMAG3 ME biodistribution using a gamma counter. Mice were imaged according to procedure and terminated at 24 hours for gamma counting of tissue samples. Body parts including lungs, heart, liver, spleen, kidney, digestive tract, brain and tumor were excised and weighed. Samples were then extracted from whole organs, weighed, and placed in 0.5 ml ethanol in counting tubes. Samples were allowed to decay an additional 33.5 hours before counting. Gamma counting was performed on a Packard Cobra II gamma counter. A NIST traceable 50 μCi (decayed to count time) ^{99m}Tc standard and a 0.5 ml ethanol background sample were counted with the tissue samples. The standard was used to determine gamma counter efficiency for the ^{99m}Tc samples (Appendix C). Counting time was 10 minutes for each sample with a 20% window around the 141 keV photopeak of ^{99m}Tc and an additional wide spectrum window. The well was set at the 0.5 ml sample position for maximum detector efficiency. Percent injected dose for gamma counter specimens at 24 hours was determined by the following procedure: CPM for the whole body region at T=0 were converted to dpm using a previously determined ^{99m}Tc efficiency for the gamma camera (Appendix D) and dpm was decay corrected to sample count time. DPM at count time for the gamma counter specimens was determined by using the gamma counter efficiency determined at counting. Finally, percent injected dose at 24 hours was determined by comparing the decay corrected gamma counter activity to the T=0 gamma camera activity (Appendix C)

3.5 Error Propagation

Error propagation for biodistribution results was determined using the standard textbook derivation (Knoll, 1979; Sorenson and Phelps, 1987) of the Taylor approximation method. A consultation with an OSU Statistics Department Research Assistant revealed that a more rigorous Taylor approximation (also known as "the Delta method") for uncertainty of the biodistribution function for

the gamma camera results was needed because the variables in the function were not entirely independent from one another. Therefore, a Taylor approximation derived from the equation by the consultant was used. Briefly, the equation was expanded about the mean of each variable to a linear equation. The variance of the linear equation was determined by taking the square of the partial derivative of the expanded equation. Uncertainty was calculated from the variance according to Knoll. For the biodistribution results from the gamma counter, error was propagated according to the derivation by Knoll and was confirmed to be the correct method by the statistics consultant since all of the observations in this function were independent. For the weighted average of the biodistribution, error was propagated according to the discussion found in Wang et al., 1975.

3.6 Health Physics Concerns/Instrumentation

Assay of radioactive solutions, doses for injection and filters for quality control was performed on a Victoreen Cal/Rad Isotope Calibrator. The dose calibrator was calibrated prior to the study using procedures found in NRC Regulatory Guide 10.8 Appendix C. NIST traceable ^{99m}Tc, ^{137}Cs and ^{57}Co standards were prepared by Oregon Central Pharmacy, Eugene, OR. In addition, a correction factor was calculated and employed for all assays of ^{99m} Tc to assure a more accurate reading. (The entire calibration procedure and accompanying data is found in Appendix E.).

Intrinsic (collimator off) 40 million count flood fields using an 18.5 MBq (500 μCi) ^{99m}Tc point source at 3 meters from the gamma camera were performed on the IS2 gamma camera prior to all imaging studies and visual analysis and NEMA calculations performed. A camera tune consisting of re-peaking the camera and acquiring energy and uniformity tables was performed prior to imaging when necessary. (The procedure for calibration of the IS2 gamma camera is found in Appendix D).

In order to determine injected dose, gamma camera efficiency was determined. Briefly, a NIST traceable 37 MBq (1 mCi) aliquot in 25 ml was drawn into a 35 ml syringe to approximate a mouse with uniform biodistribution. The syringe was then laid on the gamma camera face at 5 cm from the collimator. 9 images in a

random pattern, which included the entirety of the gamma camera useful field of view, were acquired for 1 minute each using a 512 x 512 x 16 pixel matrix. Efficiency was calculated using the resulting cpm from each image divided by the decayed syringe activity converted to dpm. The individual efficiencies were converted to an overall efficiency for the entire face of the gamma camera. (The procedure and data for the IS2 efficiency determination is found in Appendix D).

3.7 Radiation Safety

Shielding was acquired for the labeling portion of the study and included a mini benchtop table shield with lead bricks surrounding the main radioactive work area inside the fume hood. All vials and syringes containing radioactive material were shielded throughout the procedure. Syringe shields were constructed of 1/8" lead sheeting, cut to proportion and wrapped around the syringe. Vials and solutions containing radioactive materials were shielded with at least ¼" lead. Other standard radiation safety procedures and practices were employed including labeling all radioactive solutions and materials, remote handling devices, finger rings and whole body badges and post work surveys and decontamination.

Dose reconstruction for the imaging portion of the study was performed using MicroShield version 5.5 (5.05-00615). The modeled source was a simple cylinder in the dimensions of a typical mouse (height 7.62 cm, radius 1.9 cm) with 37 MBq (1 mCi) ^{99m}Tc uniformly distributed throughout. Calculation point was the middle of the cylinder at 1 cm from the mouse. Shielding material was 1.9 cm tissue (density 2.35 g/cm^3) and 1 cm air (1.22 E-3 g/cm^3). Holding time for each mouse was assumed to be 10 minutes for anesthesia and imaging and, therefore, 6 mice could be imaged per hour. The initial dose rate determined by MicroShield was decayed for each imaging time point, multiplied by a time factor, then added to determine total estimated dose to the extremities for imaging. The badges and finger rings of the primary animal handler were sent for analysis immediately following the first procedure to confirm the MicroShield reconstruction results. (See Appendix F for the dose reconstruction method and data).

Radioactive animals were allowed to decay for 24 hours post injection prior to performing necropsy. Samples were decayed an additional 24 hours and were indistinguishable from background via a direct survey before being sent for microscopic analysis.

Waste and animal parts were packaged and picked up by radiation safety immediately following the end of imaging. Post work surveys and decontamination of all work areas were performed and documented immediately following each procedure.

4.0 Results

4.1 Peptide Labeling

Radiolabeling efficiencies were 99.2%, 96.6% (^{99m}TcMAG3 ME Formula 1), 98.5% and 98.2% (^{99m}TcMAG3 ME Formula 2) for the four labeled solutions respectively.

Cold peptide quality control results performed at Gene Tools, Inc. indicated that the peptide should be eluted from the column after washing with 5 ml 5% $NaHCO_3$ however, this was not found to be the case with the ^{99m}TcMAG3 ME. The peptide remained on the column even after 30 ml of the $NaHCO_3$ solution was applied to the column. It was therefore necessary to assume that all activity remaining on the column was the ^{99m}TcMAG3 ME labeled entity.

It was determined that the peptide may not have been entirely free in the final injected solution due to aggregation of the protein molecules and this was having an effect on the sep pak column elution as well as *in*-vivo distribution of the peptide, which seemed to hang up in capillary beds near the injection site and in the lungs. The labeling method was adjusted during the 3rd and 4th procedures to encourage the peptide to remain free in solution by adding 0.5 ml 5% mannitol solution the final peptide solution (Formula 2). While the addition of mannitol to the final ^{99m}TcMAG3 ME solution had no effect on ability to elute the peptide from the column during the quality control phase, it was found that *in-vivo* distribution of ^{99m}TcMAG3 ME shifted from predominately accumulating in lungs to predominantly accumulating in the liver.

4.2 Scintigraphy Results

Scintigraphy showed that the ^{99m}TcMAG3 ME accumulated in tumor in high enough concentration to be visualized on planar gamma camera images in 5 LLC1 mice with base of tail tumors. *(Figure 4.2a).* Tumors were confirmed at necropsy and compared to pathology results except for S4M2, where pathology results were not available. For S4M2 the pattern of uptake at the base of the tail suggested a tumor was present and therefore this mouse was included in the positive results.

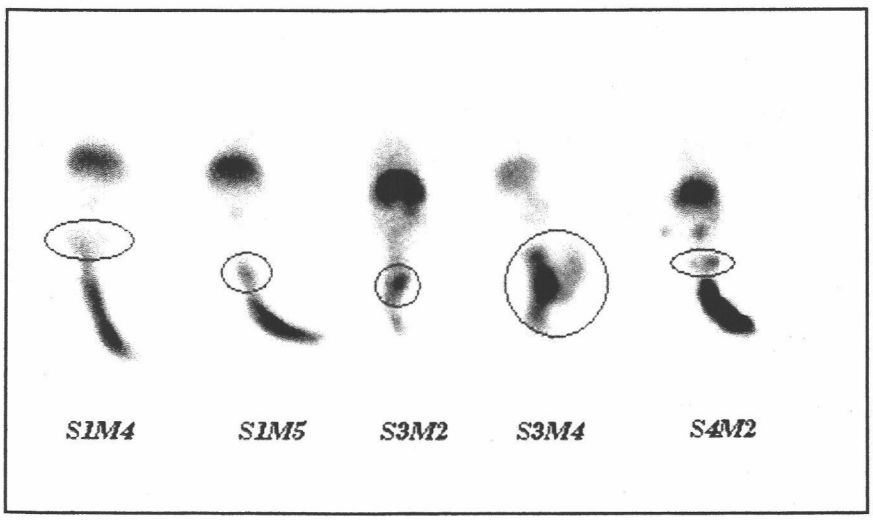

Figure 4.2.a) Tumors at base of tail visualized by planar gamma scintigraphy. 8 hour images area shown.

Tumors were seen in at least one mouse in each imaging session, except session 2, and regardless of the formulation of the ^{99m}TcMAG3 ME. No tumors were visualized in the 2nd imaging session during scintigraphy, most likely a result of not allowing the tumor cells to grow for a long enough period *in-vivo.* Conversely, the tumor cells in mice prepared for the 3rd study were allowed to grow too long and all but one of the tumor bearing mice were terminated prior to the 24 hour time point. Consequently, a time of approximately 3 weeks was determined to be a close estimation of the period required for *in-vivo* LLC1 tumor growth in the C57blk-J6 injected with Lewis Lung cells prior to gamma imaging.

Visual analysis of the free ^{99m}Tc mice images showed markedly different pharmacokinetics from either the ^{99m}TcMAG3 ME control or the ^{99m}TcMAG3 ME

mice (Figure 4.2b). The jugular injection in S4M1 removed the artifact which obscured base of tail tumor visibility, however, no activity appeared at the base of the tail indicating positive for tumor in this LLC1 mouse.

In most instances a large accumulation of activity was seen near the injection area in ^{99m}TcMAG3 ME mice with tumors and non-tumor control mice that did not clear over 24 hours. This phenomenon occurred in mice with confirmed tumors at the base of the tail and in control mice. Significantly, the free ^{99m}Tc tumor and non-tumor control images showed remarkably different *in-vivo* distribution than the ^{99m}TcMAG3 ME tumor and non-tumor control images. Areas of accumulation in the ^{99m}TcMAG3 ME mice were base of tail near injection site, tumor (5 mice), lungs and/or liver, and kidneys while accumulation for the free ^{99m}Tc images were in the thyroid, salivary glands, gastric mucosa, and bladder. In addition, there was not prolonged accumulation for the free ^{99m}Tc images near the injection site. *(Figure 4.2c)*.

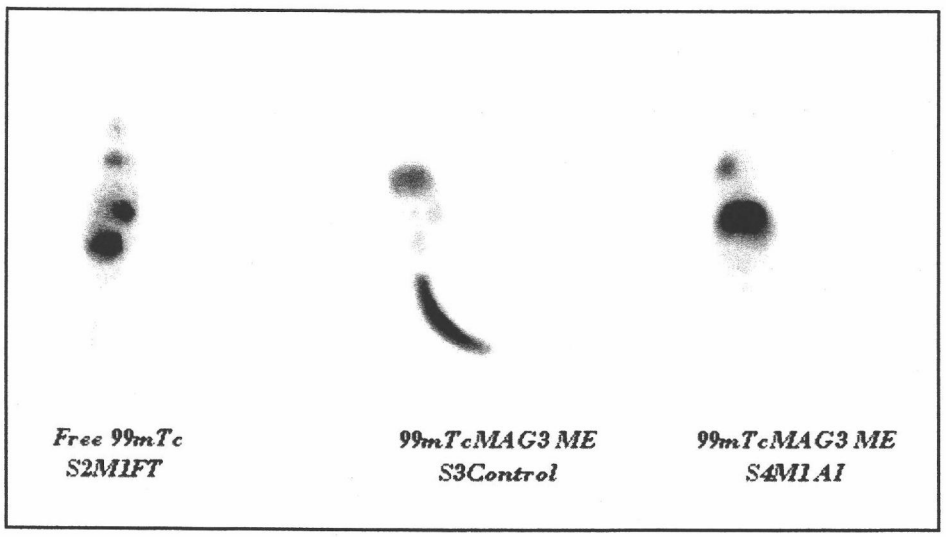

Figure 4.2b) Three Different Treatment Types. 8 hour images of three treatment types imaged during the study. The Free ^{99m}Tc mouse shows markedly different pharmacokinetics than the ^{99m}TcMAG3 ME. The aortic injection removed the injection artifact from the tail.

In addition to tumor site, the peptide showed primary accumulation in the lungs for studies 1 and 2 with a shift to primary accumulation in the liver for sessions 3 and 4 after addition of mannitol to the final labeled peptide solution *(Figure 4.2d)*.

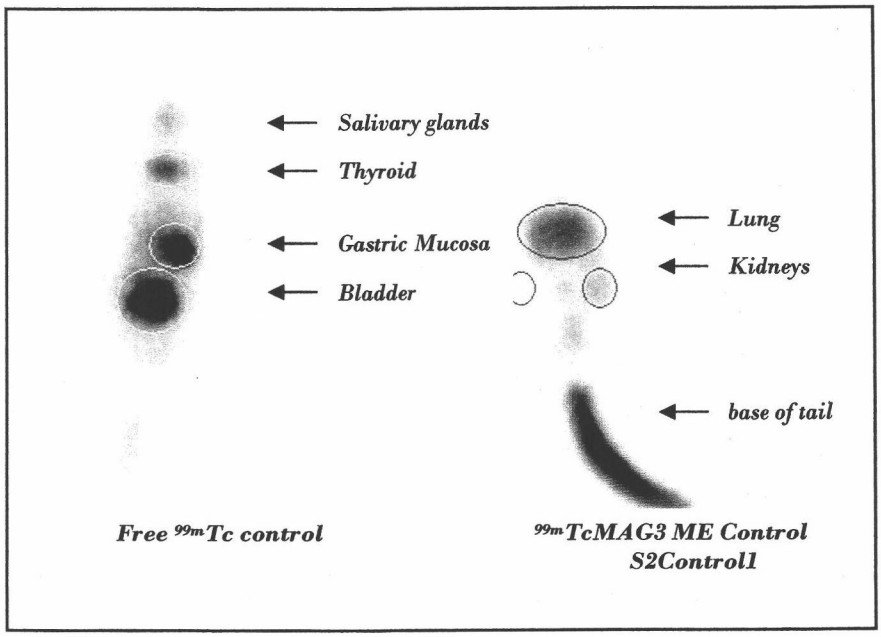

Figure 4.2c) Free ^{99m}Tc vs. ^{99m}TcMAG3peptide images. 8 hour free ^{99m}Tc and ^{99m}TcMAG3 peptide control (no-tumor) mice showing different areas of uptake for each.

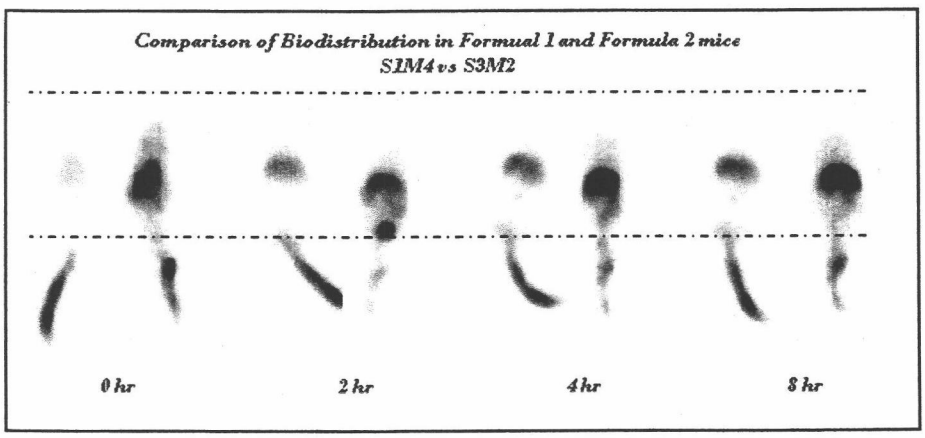

Figure 4.2d) Comparison of Biodistribution for Formula1 versus Formula 2. After addition of mannitol to the final labeling solution, primary accumulation of ^{99m}TcMAG3 ME shifted from the lungs (S1M4 on left for all time points) to the liver(S3M4 on right for all time points) . The lines in the image line up noses and bottoms of mouse bodies.

Figure 4.2e shows a complete imaging session for a tumor positive mouse from imaging session 3. The addition of mannitol to the final labeling solution shifted the primary accumulation site to the liver and a successful injection without extravasation to surrounding tissue enabled good anatomic and tumor

visualization in this subject. Lung and liver were differentiated over time as the peptide moved from the lung to the liver between 0 and 2 hours post injection for all mice in the 3rd and 4th imaging sessions.

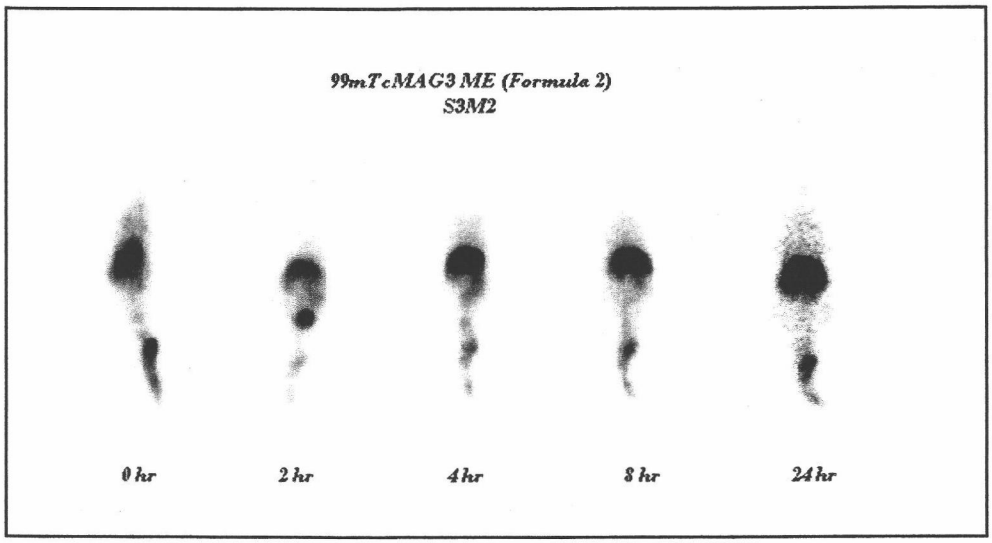

Figure 4.2e). Complete image session S3M2. 0,2,4,8,and 24 hour images (left to right) of tumor positive ^{99m}TcMAG3 peptide mouse. The addition of mannitol to the final labeling solution and good injection technique enabled peptide to move quickly through the injection site and tumor is visualized readily at all time points. In addition, the T=0 to T=2 images allow differentiation of liver from lungs.

Injection at the jugular vein improved pharmacokinetics of the peptide by allowing a more direct route for the ^{99m}TcMAG3 ME to enter circulation. Figure 4.2f shows how this technique improved image quality. Moving the injection site away from the implanted tumors should also positively affect resolution of tumor, however, a tumor was not visualized in this subject.

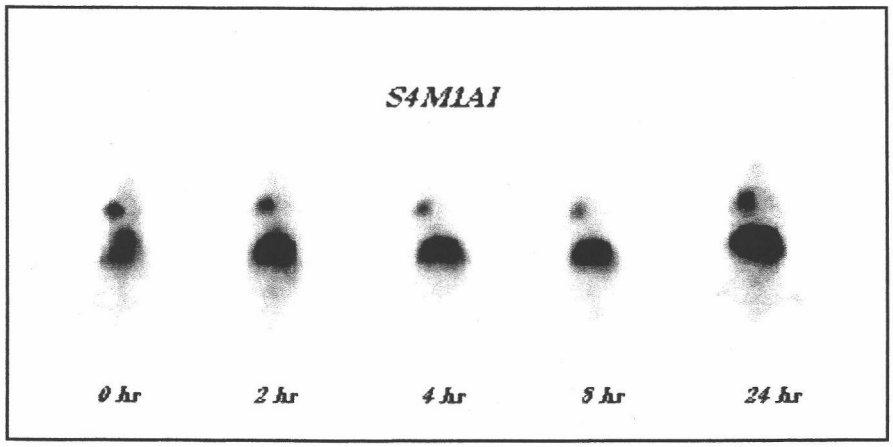

Figure 4.2f) Complete imaging session of jugular vein injected mouse.

4.3 Imaging Biodistribution Results

Biodistribution data reconstructed from regions of interest drawn on the Hermes workstation show primary accumulation from 2 to 24 hours in the lungs for the peptide in studies 1 and 2 *(Table 4.3a)* with a weighted average T_{max} of 21.4 ± 0.1 %ID at approximately 8 hours post injection. In studies 3 and 4 the lungs showed much less activity overall with the primary focus shifted from the lung in the Formula 2 mice. The Formula 2 control mouse showed a peak in activity at 9.4 %ID at 4 hours with decrease in lung activity to near 0 by 12 hours. For studies 3 and 4 the addition of mannitol to the final peptide solution effectively decreased the total concentration of ^{99m}TcMAG3 ME in the lungs. However from approximately 4 hours to 24 hours the concentration of ME in the lungs remained steady at around 2.5 %ID.

Table 4.3.a) Individual and Weighted Average Percent Injected Dose - Lungs. Individual and weighted average uptake and standard error over 24 hours for 7 mice injected with Formula 1 99mTcMAG3 ME and 5 mice injected with Formula 2 99mTcMAG3ME. (Lungs were differentiated from liver in imaging session 3 and 4.)

%Injected Dose Lungs (Formula 1 and 2)					
Mouse Number	0 hr	2 hr	4 hr	8 hr	24 hr
S1M2	12.4 ± 0.1	17.9 ± 0.1	20.5 ± 0.2	21.3 ± 0.2	
S1M4	9.5 ± 0.1	18.6 ± 0.1	21.9 ± 0.2	22.6 ± 0.2	
S1M5	9.0 ± 0.1	20.4 ± 0.1	24.3 ± 0.2	28.9 ± 0.2	
S2M1	0.2 ± 0.0	14.2 ± 0.1	20.2 ± 0.2	21.2 ± 0.2	17.4 ± 0.5
S2M2	0.5 ± 0.0	15.1 ± 0.1	19.3 ± 0.2	20.5 ± 0.2	16.0 ± 0.5
S2M3	0.4 ± 0.0	17.6 ± 0.1	16.5 ± 0.2	18.7 ± 0.2	17.3 ± 0.5
S2M4	0.5 ± 0.1	11.0 ± 0.1	14.0 ± 0.1	16.3 ± 0.2	16.0 ± 0.5
WT AVG Form 1	**4.5 ± 0.0**	**16.4 ± 0.1**	**17.9 ± 0.1**	**21.4 ± 0.1**	**16.7 ± 0.2**
S3M2	16.5 ± 0.1	6.0 ± 0.1	4.6 ± 0.1	6.4 ± 0.1	2.7 ± 0.2
S3M4	2.1 ± 0.0	1.0 ± 0.0	1.2 ± 0.0	1.7 ± 0.1	
S4M2	0.6 ± 0.0	2.7 ± 0.1	2.7 ± 0.1	2.1 ± 0.1	1.7 ± 0.2
S4M3	0.1 ± 0.0	2.4 ± 0.0	1.3 ± 0.0	1.0 ± 0.1	1.1 ± 0.2
WT AVG Form 2	**4.8 ± 0.1**	**3.0 ± 0.1**	**2.4 ± 0.1**	**2.8 ± 0.1**	**1.8 ± 0.1**
Control (Form 2)	-0.3 ± 0.0	9.4 ± 0.1	2.1 ± 0.1	0.6 ± 0.1	-0.3 ± 0.3
S4M1(JI)	20.9± 0.3	9.8 ± 0.1	5.6 ± 0.1	5.7 ± 0.1	3.3 ± 0.2

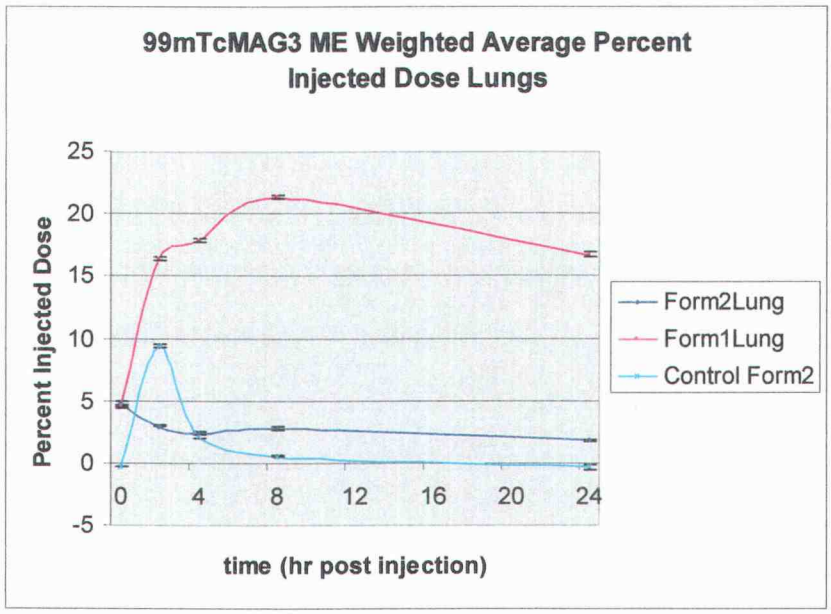

Figure 4.3.a) Percent Injected Dose Lungs. Graph shows weighted average percent injected dose in the lungs for Formula 1(n=9), Formula 2 (n=4) and Control (n=1).

Formula 2 ^{99m}TcMAG3 ME continued to concentrate over time in the liver with a weighted average T_{max} of 22.8 ± 0.4 %ID and rising at T=24. By contrast T_{max} for the AI mouse was 72 ± 0.4 %ID at 8 hours. The Formula 2 control mouse again showed a peak in activity of 31.7 ± 0.2 %ID at close to 2 hours with a near steady state in the liver at around 14% and minimal excretion by 24 hours. (Table 4.3b and figure 4.3b)

Table 4.3b) Individual and Weighted Average Percent Injected Dose - Liver.

Mouse #	%ID Liver				
	0	2	4	8	24
S3M2	40.6 ± 0.3	44.3 ± 0.2	42.5 ± 0.2	40.0 ± 0.3	41.1 ± 0.7
S3M4	6.5 ± 0.1	11.2 ± 0.1	10.2 ± 0.1	10.7 ±0.1	
S4M2	-0.2 ± 0.1	9.4 ± 0.1	16.3 ± 0.1	16.7 ± 0.2	18.9 ± 0.4
S4M3	1.2 ± 0.1	18.0 ± 0.1	14.6 ± 0.1	15.6 ± 0.2	14.4 ± 0.8
Wt AVG	**3.9 ± 0.1**	**15.3 ± 0.1**	**15.9 ± 0.1**	**14.4 ± 0.1**	**22.8 ± 0.4**
S4M1(JI)	45.3 ± 0.7	65.8 ± 0.6	70.4 ± 0.5	72.0 ±0.4	66.0 ± 0.6
Control	-0.2 ± 0.1	31.7 ± 0.2	14.2 ± 0.1	14.3 ± 0.2	11.9 ± 0.6

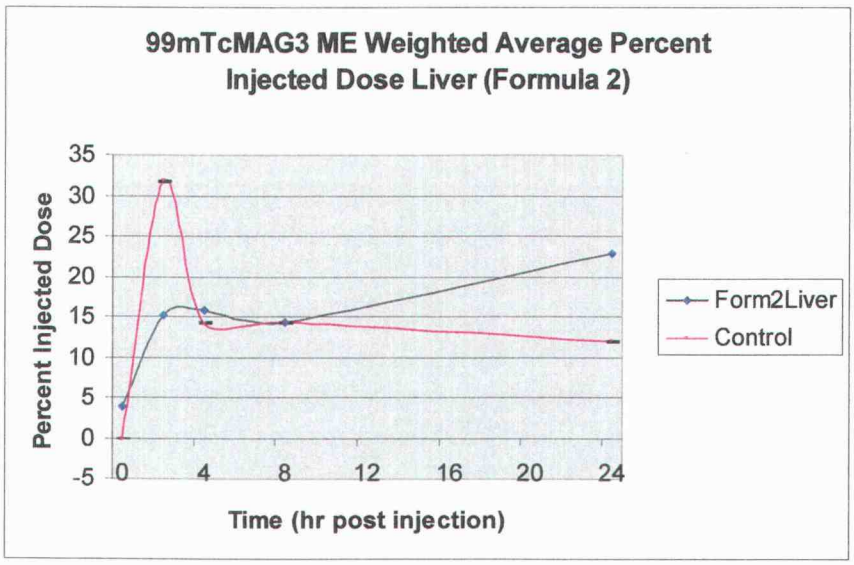

Figure 4.3b) Percent Injected Dose Liver. Graph is for weighted average Formula 2 (n = 4) and Formula 2 Control (n=1).

Individual and weighted Average %ID for 5 tumor positive mice are shown in Table 4.3c and Figure 4.3c. ^{99m}TcMAG3 ME accumulated in tumor regardless of formulation.

Table 4.3.c) Individual and Weighted Average % Injected Dose – Tumor.

	%Injected Dose Tumor (Formula 1 and 2)				
Formula 1	0	2	4	8	24
S2M4	0.7 ± 0.0	6.2 ± 0.1	3.8 ± 0.1	5.7 ± 0.1	
S2M5	4.2 ± 0.1	5.9 ± 0.1	5.0 ± 0.1	5.2 ± 0.0	
WTAVG Form1	**2.5 ± 0.1**	**6.0 ± 0.1**	**4.4 ± 0.1**	**6.3 ± 0.1**	
Formula 2					
S3M2	15.3 ± 0.2	6.0 ± 0.1	6.9 ± 0.1	7.6 ± 0.8	5.8 ± 0.0
S3M4	101.7 ± 0.4	50.6 ± 0.2	49.8 ± 0.2	54.8 ± 0.3	
S4M2	0.1 ± 0.0	0.9 ± 0.1	2.4 ± 0.1	2.6 ± 0.1	2.3 ± 0.1
WTAVG Form2	**7.8 ± 0.1**	**8.7 ± 0.1**	**9.6 ± 0.1**	**7.8 ± 0.1**	**2.4 ± 0.1**
WT AVG Form 2 (S3M4 excluded from calc)	**3.0 ± 0.1**	**3.5 ± 0.1**	**4.6 ± 0.1**	**2.6 ± 0.1**	**2.4 ± 0.1**

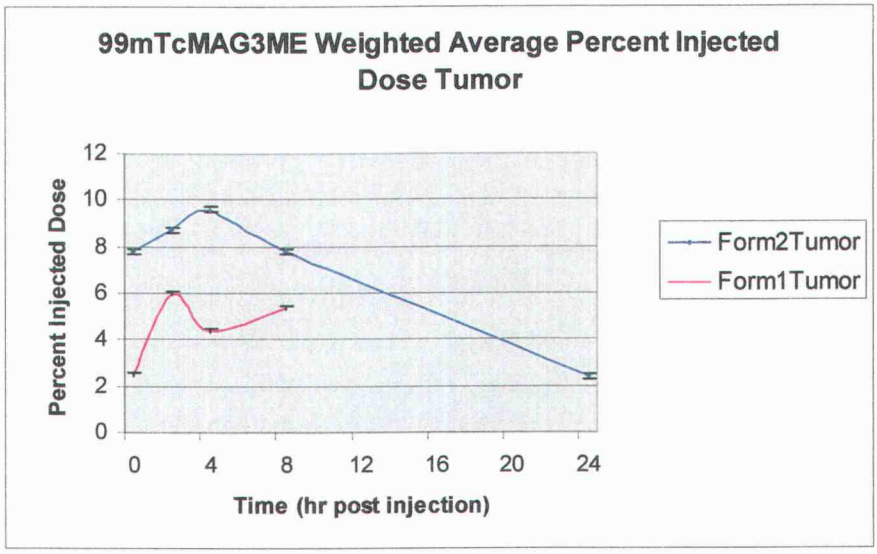

Figure 4.3c) Percent Injected Dose Tumor. Weighted average %ID for mice injected with 99mTcMAG3 ME formula 1 (n=2) and formula 2 (n=3) and positive for base of tail tumors by gamma scintigraphy.

Mouse number S3M4 is anomalous, assuming that tumor uptake results were obscured because the tumor was allowed to grow to near the size of the mouse. Interestingly, uptake in the lungs and liver of S3M4 was close to the norm for mice injected with formula 2 ^{99m}TcMAG3 ME. Figure 4.3d represents Formula 2, excluding S3M4, compared to Formula 1 tumor biodistribution.

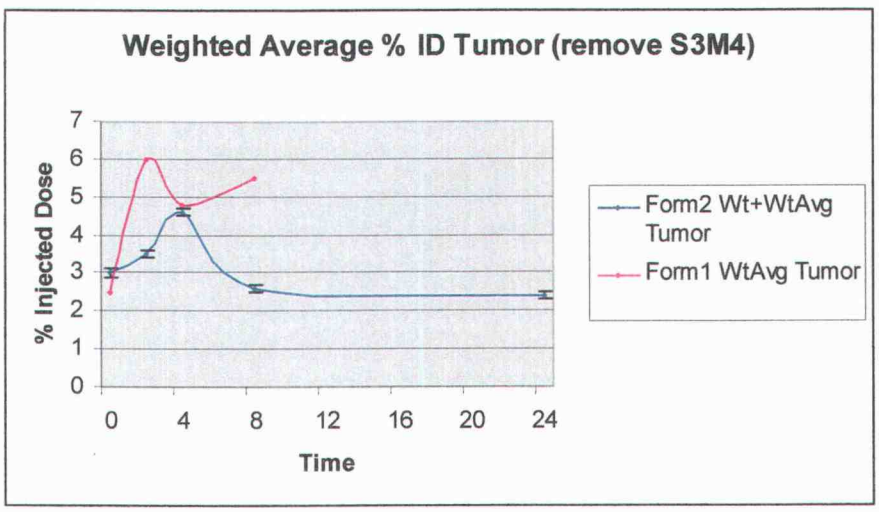

Figure 4.3d) Tumor biodistribution excluding the anomalous S3M4 which showed uptake much larger than the norm.

4.4 Gamma Counter Biodistribution Results

24 hour % ID calculated from gamma counting results in the 3rd study showed some uptake in all organs except the brain and heart. Table 4.4a and Figure 4.4a show results for 24 hour % ID by gamma counter method.

Table 4.4a) Gamma Counter Method 24 hr % ID for 99mTcMAG3 ME tumor positive and control mice.

	24 hr %ID S3M2	24 hr %ID S3 Control
Lungs	2.2 ± 2.2	0.2 ± 0.1
Heart	0.2 ± 0.1	0.1 ± 0.01
Liver	34.5± 2.7	11.7 ± 10.5
Spleen	1.2 ± 0.2	0.3 ± 0.1
Kidney	6.5 ± 0.4	2.8 ± 0.2
Digestive Tract	6.5 ± 0.3	1.5 ± 0.91
Brain	0.04 ± 0.01	0.01 ± 0.01
Tumor	13.0 ± 0.8	

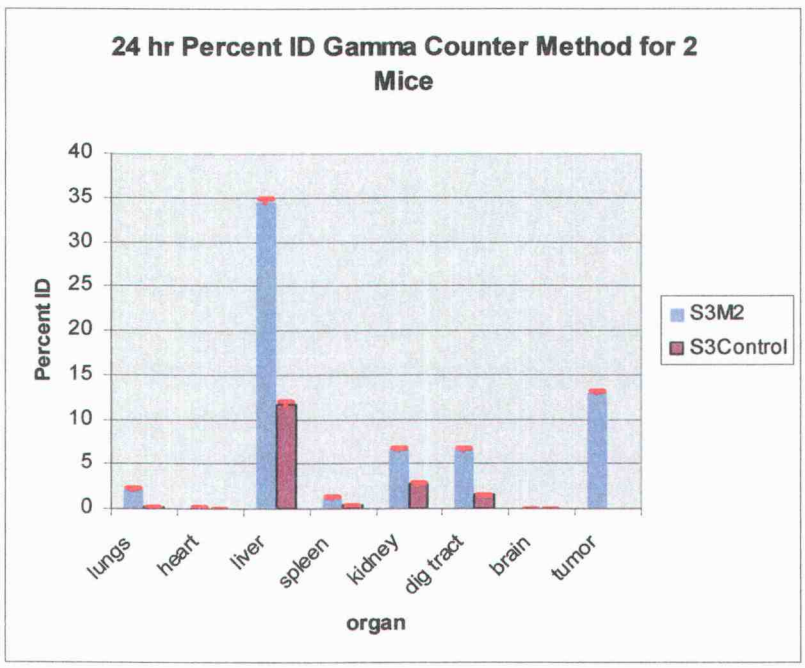

Figure 4.4a) Percent Injected Dose by Gamma Counter. 24 hour % ID in selected organs for 2 mice from study 3 shows accumulation of 99mTcMAG3 ME in tumor, liver, digestive tract, kidney, lungs and spleen.

For the tumor positive ^{99m}TcMAG3 ME mouse at 24 hours post injection, tumor activity was 13.0 ± 1.4 %ID and the liver showed the highest accumulation at 34.5 ± 4.0 %ID. Interestingly, the lungs showed minimal activity at 24 hours for the control mouse (0.2 ± 0.1 %ID), while the ^{99m}TcMAG3 ME LLC1 (S3M2) mouse was positive for activity (2.2 ± 2.2 %ID) in the lungs at 24 hours. S3M2 was positive for lung metastasis at necropsy. Some ^{99m}TcMAG3 ME was also present in the digestive tract, kidneys and spleen, with minimal activity in heart and brain for both mice. % ID in the tumor positive mouse was at least double the control %ID at 24 hours for all organs.

Figure 4.4b shows a comparison of the gamma camera results to the gamma counter results for biodistribution in S3M2 and the S3 Control mouse. Good correlation was seen between the two methods, although the tumor showed the highest discrepancy at 12.9 ± 1.4 verses 5.8 ± 0.1 24 hour %ID for gamma counter and gamma camera, respectively.

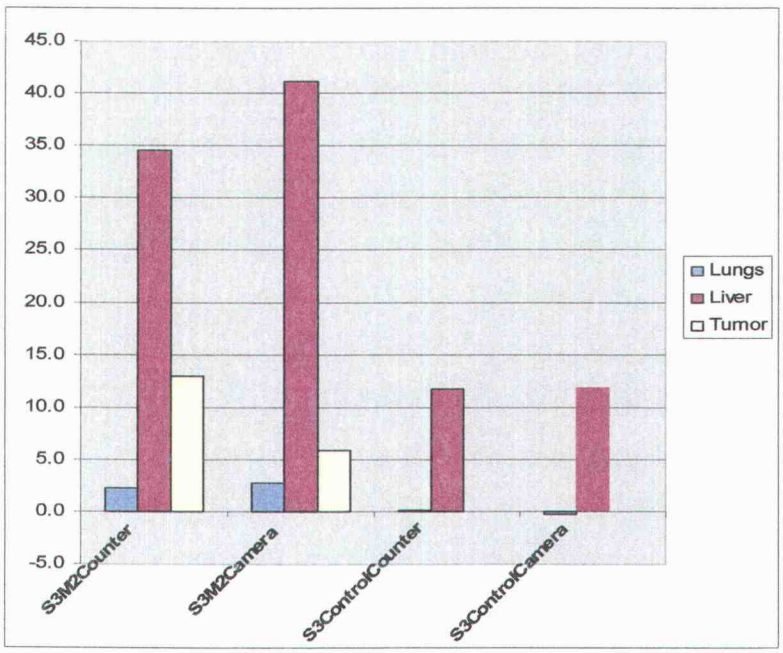

Figure 4.4b) Comparison of results between gamma counter and gamma camera method.

A student's paired t test was performed which found these results were not statistically significant (p=0.994 for S3M2 and 0.99 for S3Control). Table 4.4c shows a comparison of the results between the two methods.

Table 4.4c) Comparison and % ID for gamma camera verses gamma counter results.

	S3M2		S3 Control	
	Counter	Camera	Counter	Camera
Lungs	2.2 ± 2.2	2.7 ± 0.1	0.2 ± 0.1	-0.3 ± 0.1
Liver	34.5 ± 2.7	40.1 ± 0.3	11.7 ± 0.5	11.9 ± 0.6
Tumor	13.0 ± 0.8	5.8 ± 0.0		
P value	0.994		0.994	

5.0 Discussion

The pH activated molecular engine described in this study may be useful for diagnosis and therapy of different types of cancer. It was shown that the pharmacokinetics were markedly changed *in-vivo* from that expected by either free ^{99m}Tc or ^{99m}TcMAG3. Tumor was visualized in 5 mice positive at necropsy for base of tail tumors indicating the molecular engine was capable of delivering a chelated molecule to the surface of tumor cells. Results of tumor uptake may have been obscured by the large size of the tumor on mouse S3M4, therefore, biodistribution was calculated for Formula 2 mice and excluding S3M4. This is more likely a more realistic picture of the Formula 2 biodistribution. Tumor uptake showed a peak between 2 and 4 hours at 2.5 ± 0.1% near 2 hours for Formula1 mice, 7.8 ± 0.1% near 3.5 hours for Formula 2 mice and 3.0 ± 0.1% for Formula 2 (S3M4 excluded). It appeared that concentration of ME in the tumor was dropping steeply by 4-8 hours for Formula 2 while the concentration seemed to stay in a more or less steady state until 8 hours for formula 1. This is could be a result of the ME aggregation within capillary beds in the tail of the Formula 1 mice. From 8-24 hours, the concentration of ME stayed fairly steady in the formula 2 mice while it is impossible to tell what may have happened to the ME during this period for the Formula 1 mice since they were only imaged to 8 hours.

In imaging session 1 and 2 ^{99m}TcMAG3 ME accumulated primarily in the lungs, and the lungs could not be differentiated from the liver The lungs were differentiated from the liver in imaging sessions 3 and 4 and were small compared to the liver. The change in distribution is most likely an effect of adding mannitol to the final labeling solution in studies 3 and 4 to prevent the peptide from aggregating to other peptide molecules and hanging up in capillary beds. This change and resulting biodistribution curves indicating primary accumulation in the liver for imaging sessions 3 and 4 is thought to provide a more accurate visualization of the expected whole body distribution for ^{99m}TcMAG3 ME.

For the lungs and liver the control mice had faster pharmacokinetics than the ^{99m}TcMAG3 ME mice. The S3Control mouse showed a spike of activity in both the liver and lungs at approximately 2 hours post injection which leveled off at approximately 4 hours post injection and excreted slowly up to the 24 hour end point.

This dual phase excretion curve was not apparent in the tumor positive ^{99m}TcMAG3 ME mice which showed a more prolonged uptake and excretion in both lungs and liver. The ^{99m}TcMAG3 ME mice did not show the activity spike at two hours that the S3control mouse did (31.7 verses 12.0 %ID, liver, and 9.8 versus 1.9% ID, lungs for the control mice and Formula 2 ^{99m}TcMAG3 ME mice respectively). In addition, for the Formula 2 ^{99m}TcMAG3 ME mice, the liver continued to increase in activity up to the 24 hour endpoint, while the S3 control mouse slowly decreased. The anomalies in these curves are most likely due to compromised integrity of organs and circulatory system from the malignancies. The fact that the lungs continued to concentrate ^{99m}TcMAG3 ME higher than the control over 24 hours can also be explained by the number of Formula 2 ^{99m}TcMAG3 ME mice positive for lung metastesis at necropsy (n=2), which would indicate the molecular engine is capable of routing to metastesis away from primary tumor.

While it is apparent that the pH activated molecular engine described in this study may be useful for diagnosis and therapy of different types of cancer, a number of significant areas of improvement and development can be identified.

The gamma camera images were able to resolve large organs with high concentrations of ^{99m}MAG3 ME. However the data from the gamma counter analysis probably show more precisely where the peptide was accumulated 24 hours after injection. A comparison via paired t-test ($p=0.99$) of gamma camera versus gamma counter technique for organs that were visualized by planar images showed the data from this comparison could not be correlated based on likeness of results. Intuitively, the gamma counter results should be more accurate based on the higher counting efficiency for ^{99m}Tc and lower inherent uncertainty of the gamma counting system over the imaging system.

Image resolution could be improved for the gamma camera by using a pinhole collimator for planar images or single photon emitted computer tomography (SPECT) acquisition with 3D reconstruction. The planar images were acquired in a large enough matrix to allow enlargement sufficient to draw regions of interest. However, it was very difficult to differentiate the liver from the lungs in the images. Many organs

that showed significant uptake via the gamma counter method were not resolved with planar scinitigraphy. Using SPECT to image the mice would allow differentiation and better resolution for all organs.

The ultimate choice of ^{99m}TcMAG3 as the ligand for the molecular engine was based largely on prior work by Hnatowich and Ruskcowski. The molecular engine peptide was labeled rapidly in just a few steps with only minor modifications to the procedure. In addition, the peptide was produced with labeling efficiencies greater than 90% in all cases. It is uncertain whether the final labeled solution was 100% of the desired ^{99m}TcMAG3 ME entity since a gradient elution was not performed with good results. This was due most likely to the wrong choice of solvent for the peptide elution phase or the wrong choice of column for the stationary phase and the ^{99m}TcMAG3 was never released from the column. Alternatively, the conditions of the radiolabeling process may have changed the action of the peptide on the column thereby preventing release. The labeled peptide should be subjected to HPLC with the proper choice of stationary and mobile phases or mass spectrometry for more accurate analysis of percent labeled molecular engine versus other impurities. A separation technique to remove free ^{99m}Tc and other impurities could also be employed to provide more accurate biodistribution curves for the molecular engine. A separation using a small pore filter would also fully eliminate large aggregates of peptide.

Poor tail vein injection technique and the tumors being implanted at the base of the tail obscured results in mice that were positive for base of tail tumors, which is probably the most confounding problem encountered in this study. The intensity at the injection site of the ^{99m}Tc MAG3 peptide, which did not dissipate significantly over time, created uncertainty as to the extent of tumor tissue visualized. While markers where used during acquisition to differentiate injection site from tumor, it was nevertheless difficult while drawing regions of interest to differentiate tumor from aggregated peptide in capillary beds or injection site. In addition, the choice of tail vein injection site, which traveled through the tumor at the base of the tail, may have altered uptake pattern and concentration in the tumor in favor of higher and faster accumulation. A technique that removes the injection site from the vicinity of the implanted tumor such as the jugular injection in imaging session 4 should be

employed in future studies. Larger animal models should also be considered for ease of injection and better image resolution of larger organs with planar scintigraphy.

Future research should include HPLC or mass spectrometry separation technique for the labeled peptide entities in the final solution, use of injection techniques that move the injection site away from tumor, an imaging system that will provide higher resolution for images, more data using the gamma counter method, larger animal models and new iterations of the peptide and ligand. New iterations of the pharmaceutical should explore ways to reduce molecular engine accumulation in the liver to avoid toxicity during therapy.

6.0 Conclusion

The molecular engine developed and characterized during the course of this project was successfully labeled with ^{99m}Tc via a MAG3 chelating molecule. Nuclear imaging showed the compound was able to bind to tumor tissue in concentrations high enough to be visualized in 5 of the 12 C57blk-6J tumor bearing mice in this study.

This is the first instance of success of a molecular imaging technique using the pH gradient between hypoxic tumor cells and normal tissue to attract a ^{99m}Tc labeled peptide to the tumor cell membrane. This technology has tremendous potential for highly specific medical intervention at the molecular scale and may provide an option, not only for diagnosis and treatment using nuclear medicine, but for delivery of custom nano-therapeutics which are currently being developed.

Bibliography

Fiola, C. (2003). Monoclonal Antibodies as Anticancer Agents. *US Pharmacist,* Vol. No. 28:10

Henkin, R. (2001). The Growing Use of Antibodies and Peptides in Nuclear Medicine. *NucMedNet Online Physician's Guide,* www.nucmednet.com/monopeps.pdf

Rollo, FD. (2003). Molecular Imaging and Nuclear Medicine: expectations and requirements, *MEDICAMundi* 47/1, pp 10-16.

Gillies RJ (2002) In vivo Molecular Imaging. *J. Cell. Biochem.* (suppl) 39: pp 231-238.

Wilke-Hooley J, Van den Berg A, Van der Zee J, Reinholds H. (1985). Human Tumour pH and its Variation. *Eur J Cancer Clin Oncol,* Vol. 21, No. 7, pp 785-791.

Radiopharmacy Inc. Website, http://www.radiopharmacy.com/product.shtml

Langer M, Beck Sickenger AG. (2001). Peptides as Carrier for Tumor Diagnosis and Treatment. *Curr Med Chem Anti-Canc Agents.* May;1(1): pp 71-93.

Anderson CJ. (2001). Metabolism of Radiometal-Labeled Proteins and Peptides: What are the Real Radiopharmaceuticals *in-vivo*? *Cancer Biotherapy and Radiopharmaceuticals.* Volume 16, Number 6, pp 451-455.

Rusckowski M, Qu T, Gupta S, Ley A, Hnatowitch D. (2001). A Comparison in Monkeys of ^{99m}Tc Labeled to a Peptide by 4 Methods. *The Journal of Nuclear Medicine,* Vol. 42, No. 12, pp 1870-1877.

Schirrmacher R, Comagic S, Schirrmacher E, Rosch F. (2004) Synthesis of a technetium-99m labeled L-tyrosine derivative with the *fac*-^{99m}Tc(I)$(CO)_3$-core. *Journal of Labelled Compounds and Radiopharmaceuticals.* Volume 47, Issue 8, pp 477-483.

Waibel R, Alberto R, Willuda J, Finnern R, Schibli R, et al. (1999). Stable one-step technetium-99m labeling of His-tagged recombinant proteins with a novel Tc(I)-carbonyl complex. *Nature Biotechnology.* Vol 17, pp 897-901.

Alberto R, Schibli R, Egli A, Schubiger A. (1998) A Novel Organometallic Aqua Complex of Technetium for the Labeling of Biomolecules: Synthesis of $[^{99m}Tc(OH_2)_3(CO)_3]+$ from $[^{99m}TcO_4]-$ in Aqueous Solution and Its Reaction with a Bifunctional Ligand.

Yang D, Kim D, Schechter N, et al. (2002) Assessment of Antiangiogenic Effect Using ^{99m}Tc-EC-Endostatin. *Cancer Biotherapy and Radiopharmaceuticals.* Vol. 17, No. 2, pp233-246(14).

Verbruggen A, Nosco D, Van Nerom C, Bormans G, Adriaens P, DeRoo M. (1992) Technetium-99m-L,L-Ethylenedicysteine: A Renal Imaging Agent. I. Labeling and Evaluation in Animals. *Journal of Nuclear Medicine.* 33:551-557.

Taylor A, Hansen L, Eshima D, Malveaux E, Folks R, Shattuck L, Lipowska M, Marzilli LG. (1997) Comparison of technetium-99m-ll-EC isomers in rats and humans. *Journal of Nuclear Medicine.* 38(5):821-6

Liu G, Mang'era K, Liu N, Gupta S, Rusckowski M, Hnatowich, D. (2002) Tumor Pretargeting in Mice Using (99m)Tc-Labeled Morpholino, A DNA Analog. *Journal of Nuclear Medicine.* .43(3):384-391

Zhang YM, Liu N, Zhu ZH, Ruskowski M, Hnatowich DJ. (2000) Infuence of different chelators (HYNIC, MAG3 and DTPA) on tumor cell accumulation and mouse biodistribution of technetium-99m labeled to antisense DNA. *European Journal of Nuclear Medicine.* 27(11):1700-7.

Hnatowich DJ, Qu T, Chang F, Ley AC, Ladner RC, Rusckowski M. (1998) Labeling Peptides with Technetium-99m Using a Bifunctional Chelator of N-Hydroxysuccinimide Ester of Mercaptoacetyltriglycine. *Journal of Nuclear Medicine.* 39:56-64.

Grace Vydac®. (2002) The Handbook of Analysis and Purification of Peptides and Proteins by Reversed-Phase HPLC. www.gracevydac.com

IAEA. (2001). ^{99m}Tc labeled peptides for imaging of peripheral receptors. Final report of a co-ordinated research project 1995-1991.

Fang YS, Ming Y, Jun Z, Yu SZ, Xiang ZL, Gang DQ. (2003) Can Tumor Uptake Tc-99m MDP? *Alasbimn Journal.* Year 5, No 19.

©IS2 Medical Systems SC/SR Operators Manual, Revision D

NIST (2003) "Measurement Process Characterization Handbook", Ch 2.5, www.itl.nist.gov/div898/handbook/mpc/section5/mpc55.htm

Wittke J. 1997-2003. Propagation of Errors. http://jan.ucc.nau.edu/~wittke/Microprobe/Statistics-Error.html

Wang C, Willis D, Loveland W. (1975). *Radiotracer Methodology in the Biological, Environmental and Physical Sciences.* p306-307. Prentice Hall Biological Science Series.

NRC Regulatory Guide 10.8, Appendix C, Revision 2, 1987. http://www.nrc.gov/reading-rm/doc-collections/reg-guides/general/active/10-008/

Traylor James. University of Kansas Medical Center, Nuclear Medicine, Teaching Files: http://www.rad.kumc.edu/nucmed/
permission on file 08/08/2005.

Cottin Y, Berriolo A, Guy F. (1999) "Somatostatin-Receptor Scinitgraphy Identifies a Cardiac Pheochromocytoma". *Circulation.* 100:2387-2388 Lippincott Williams & Wilkins
Permission on file 08/08/2005.

http://www.scalenet.com/ohaus/scout2.html for specs on scout SP2020 digital scale.

APPENDICES

Appendix A – Raw Images

A.1) Imaging Session 1

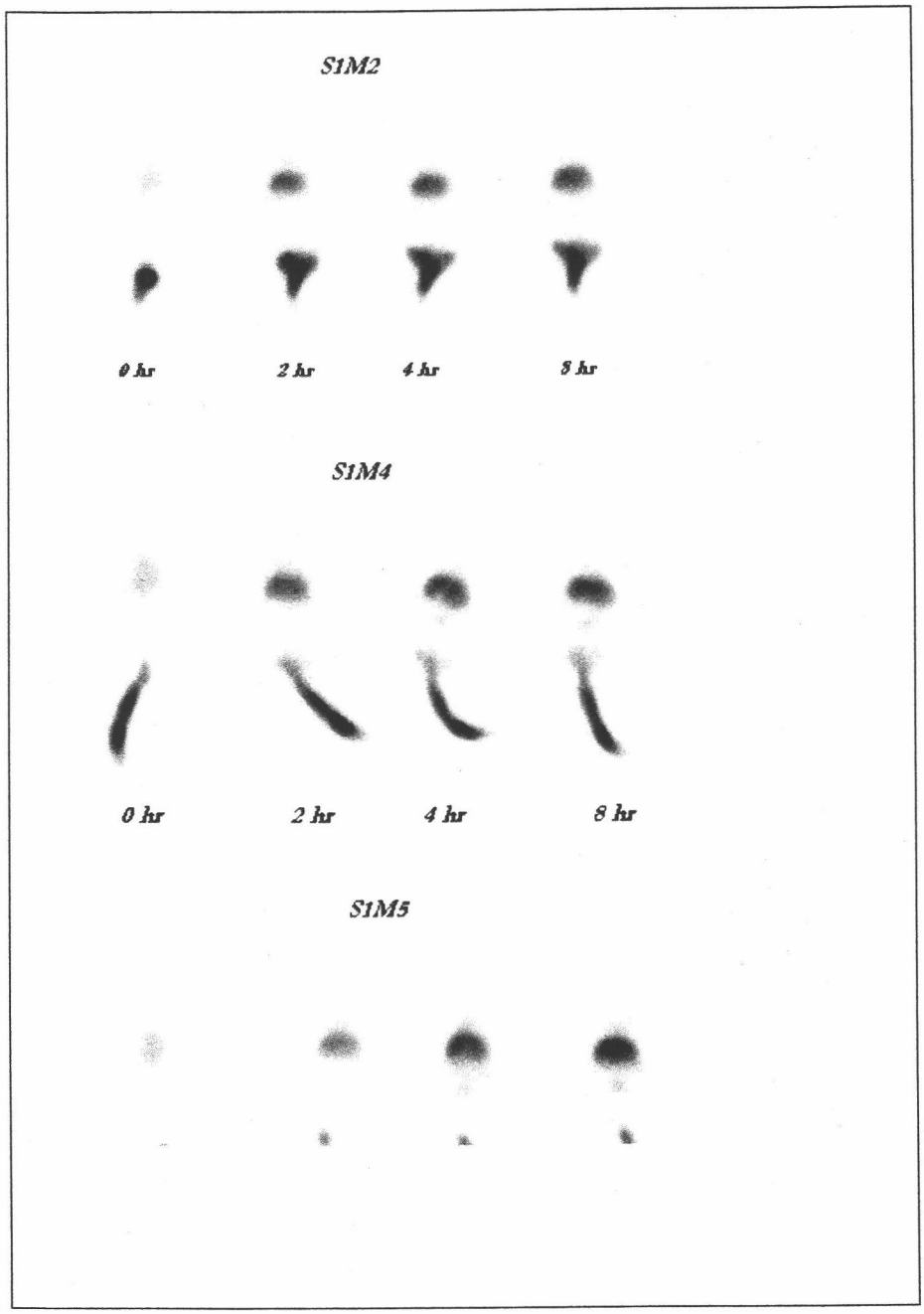

Image A.1a) Image Session 1. All mice injected with 37MBq (1mCi) Formula 1 (no Mannitol) 99mTcMAG3 ME.

Appendix A – Images

A.2) Imaging Session 2

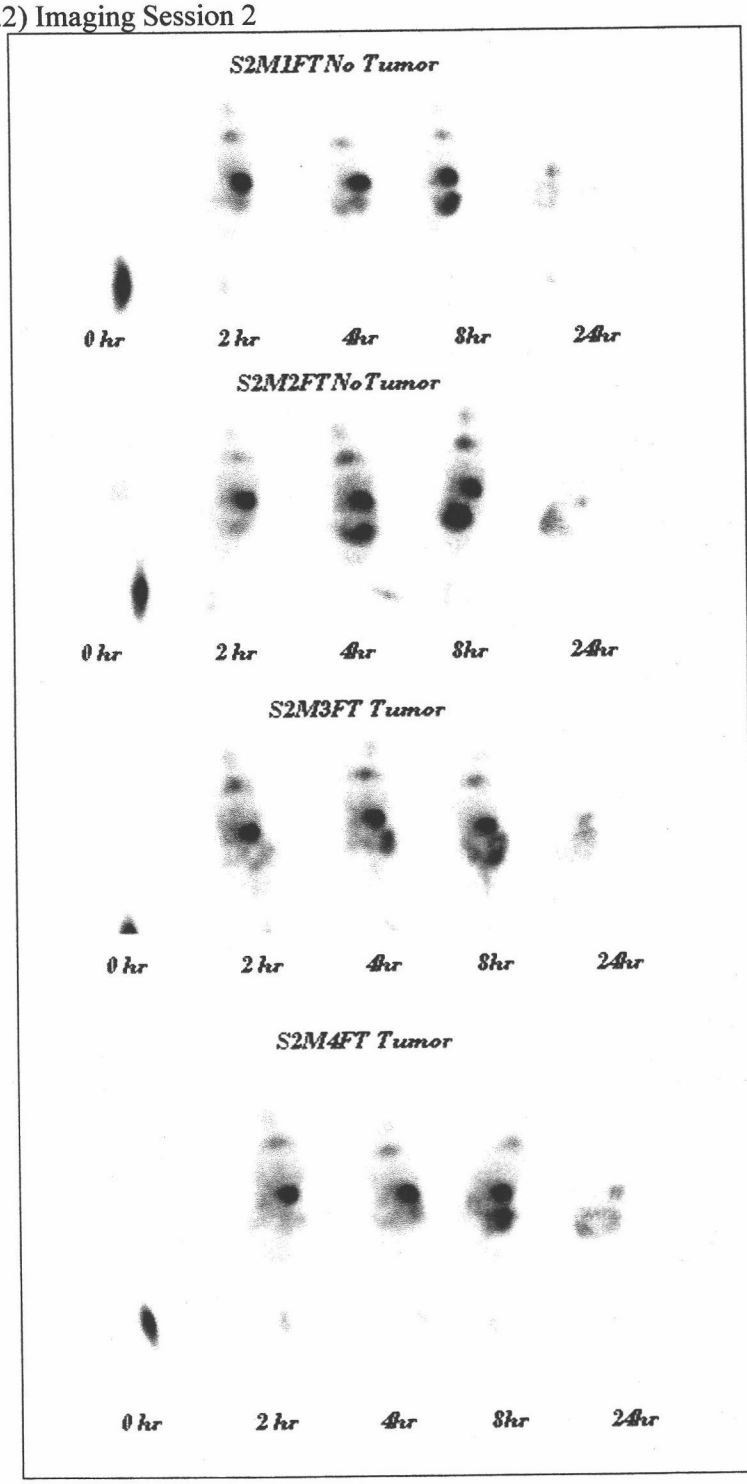

Image A.2a) Image Session 2 Free ^{99m}Tc Tumor and Non-tumor controls. All mice injected with 37 MBq (1 mCi) ^{99m}Tc pertechnetate.

Appendix A – Images

A.2) Imaging Session 2

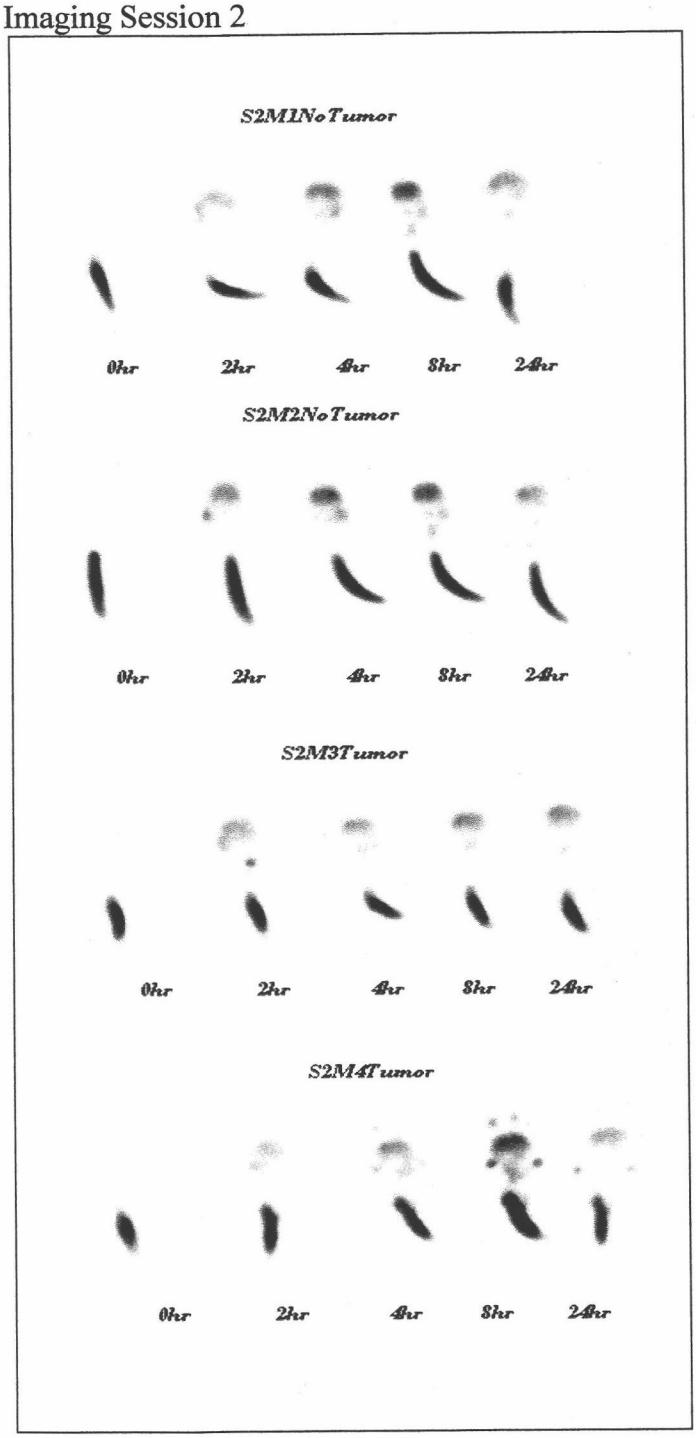

Image A.2b) Image Session 2. ^{99m}TcMAG3 ME non-Tumor Control and tumor mice in second imaging session. All mice injected with 37MBq (1 mCi) Formula 1 (no mannitol) ^{99m}TcMAG3 ME

Appendix A – Images

A.3) Imaging Session 3

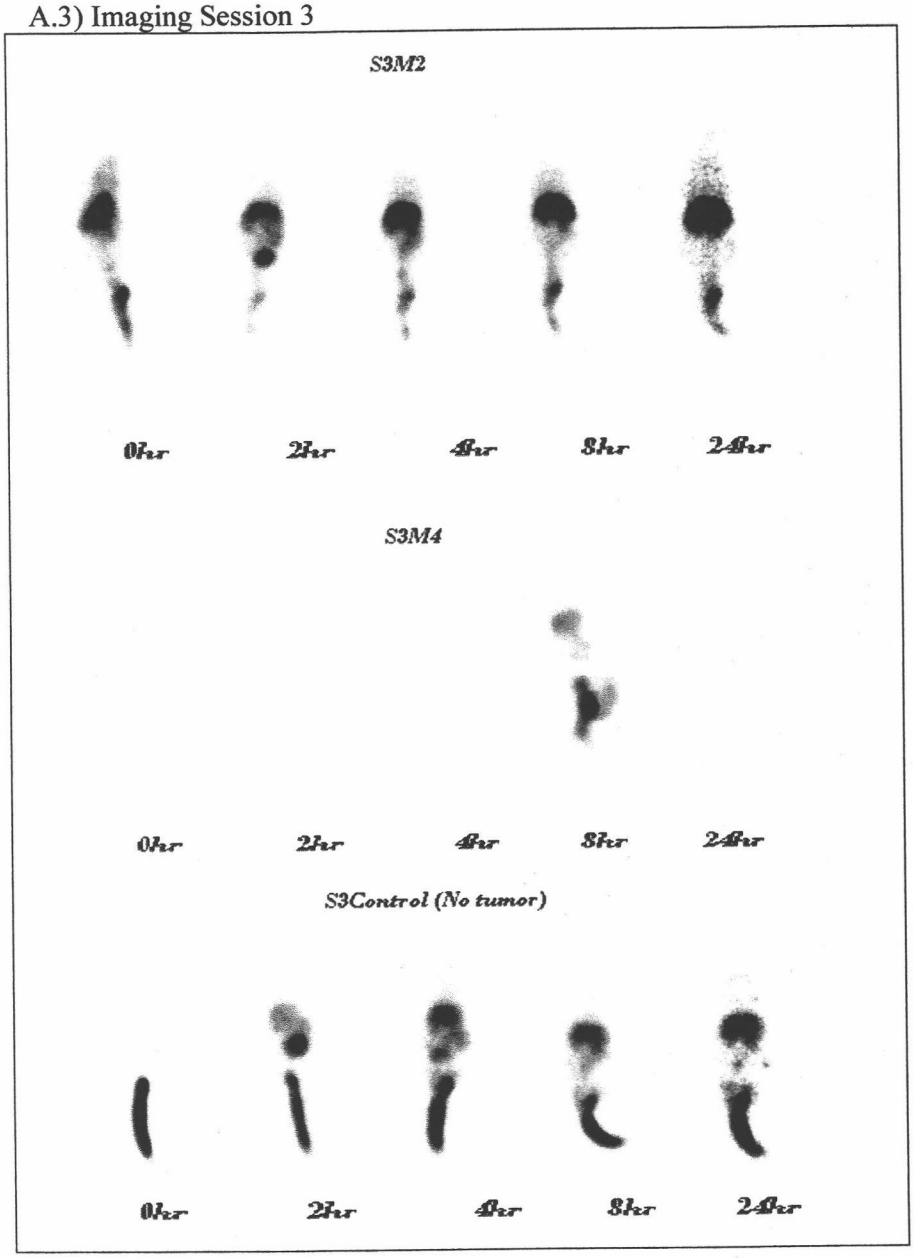

Image A3a) Image Session 3. Images of 2 tumor and 1 no-tumor control mice from 3rd imaging session. All mice were injected with 37 MBq (1mCi) Formula 2 (+ mannitol) ^{99m}TcMAG3 ME.

Appendix A – Images

A.4) Imaging Session 4)

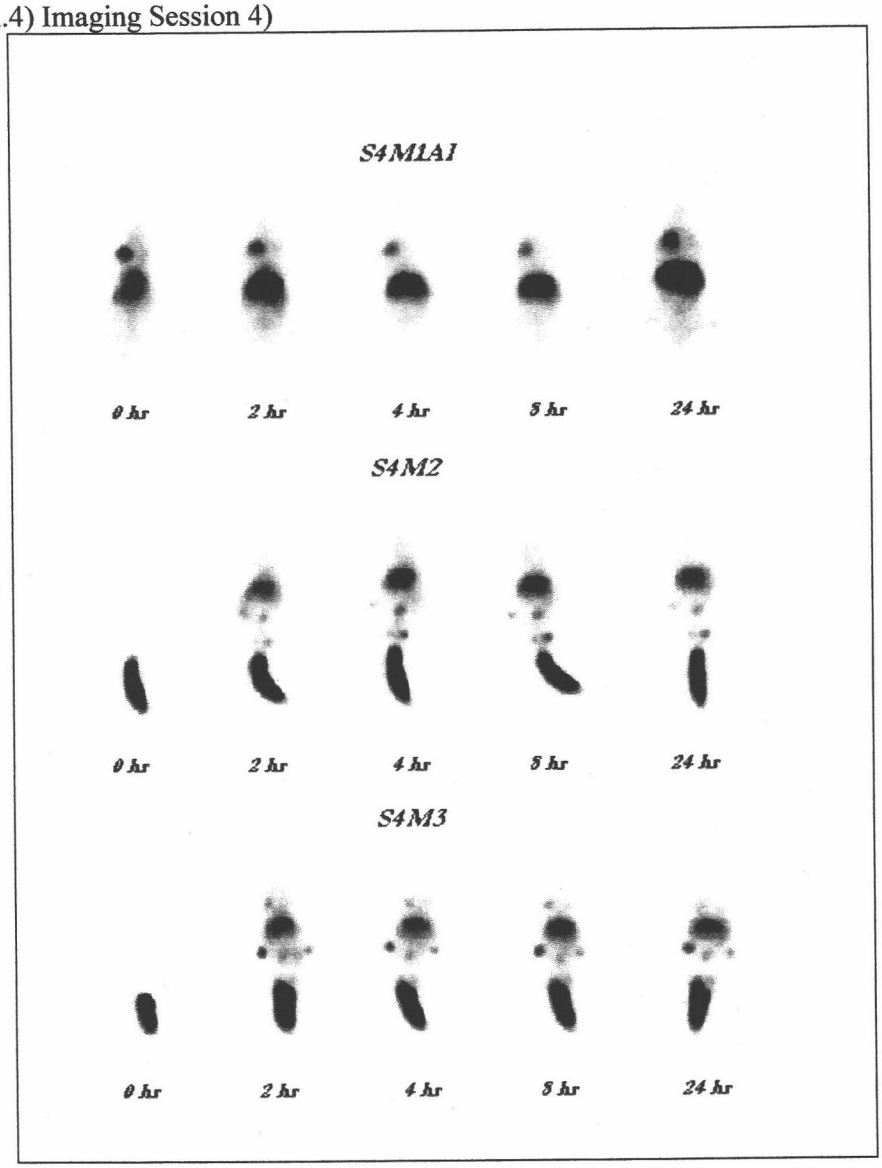

Image A.4a) Image Session 4. Mice from 4th imaging session, 2 tumor mice and 1 jugular vein injected tumor mouse. All mice were injected with 37MBq (1mCi) Formula 2 ^{99m}TcMAG3 ME.

Appendix B- Raw Data

B.1)Imaging Session 1

Table B.1a. Raw Data for 1st Imaging Session. Total raw counts per background, whole body, organ and number of cells per each area for 2nd imaging session. The lungs could not be separated from the liver and no images were positive for tumor.

time	Mouse Scint1	Image time (min)	BKG Total	#Cells BKG	WB Total	#Cells WB	Lungs Total	#Cells Lungs	Tumor Total	#Cells Tumor
0	2	2	1290	215	404372	2200	55571	911		
2	2	2	1720	215			64681	911		
4	2	4	2580	215			115697	911		
8	2	5	3010	215			98388	911		
0	4	2	860	215	336424	2200	35529	911	5103	647
2	4	2	860	215			53749	911	19245	647
4	4	4	1720	215			100210	911	21392	647
8	4	5	1505	215			81990	911	23784	647
0	5	2	1290	215	422536	2200	43728	911	21199	600
2	5	2	860	215			71969	911	22054	600
4	5	4	1720	215			136650	911	31606	600
8	5	5	1075	215			125718	911	24995	600

Appendix B- Raw Data

B.2)Imaging Session 2

Table B.2a Raw Data for 2nd Imaging Session. Total raw counts per background, whole body, organ and number of cells per each area for 2nd imaging session. The lungs could not be separated from the liver and no images were positive for tumor.

time	Mouse Scint2	Image time (min)	BKG Total	#Cells BKG	WB Total	#Cells WB	Lungs Total	#Cells Lungs
0	M1	5	354	35	719854		3826	251
2	M1	5	755	35			84220	251
4	M1	5	343	35			91170	251
8	M1	5	342	35			61309	251
24	M1	20	138	35			31545	251
0	M2	5	325	35	699328	2200	5479	251
2	M2	5	461	35			84754	251
4	M2	5	364	35			85351	251
8	M2	5	372	35			57890	251
24	M2	20	121	35			28125	251
0	M3	5	291	35	699922	2200	5090	251
2	M3	5	525	35			98865	251
4	M3	5	792	35			76724	251
8	M3	5	527	35			54429	251
24	M3	20	135	35			30598	251
						2200		
0	M4	5	346	35	626564		5416	251
2	M4	5	682	35			57627	251
4	M4	5	569	35			57377	251
8	M4	5	390	35			42063	251
24	M4	20	207	35			25755	251

Appendix B- Raw Data

B.3)Imaging Session 3

Table B.3a) Raw Data for 3rd Imaging Session. Total raw counts per background, whole body, organ and number of cells per each area for 3rd imaging session.

time	Mouse Scint3	Image time (min)	BKG Total	#Cells BKG	WB Total	#Cells WB	Liver Total	#Cells Liver	Lungs Total	#Cells Lungs	Tumor Total	#Cells Tumor
0	S3M2	2	804	42	299009	2200	112897	449	45725	166	43773	235
2		5	854	42	491321		234971	449	34019	166	35401	235
4		5	292	42	300409		175160	449	19816	166	29419	235
8		5	211	42	187060		104420	449	17107	166	20535	235
24		10	130	42	57993		34546	449	2696	166	5430	235
0	S3M4	2	824	48	383935	1950	23271	187	7754	72	313671	533
2		5	2202	53			76465	203	9216	83	329420	513
4		5	1528	44			54421	142	8176	63	254045	378
8		5	666	43			35000	153	6381	87	174894	495
0	S3Cont	2	324	42	404208	2143	2664	449	131	166		
2		5	921	42	710452		247489	449	74138	166		
4		5	586	42	314512		90552	449	14790	166		
8		5	680	42	189503		60778	449	4858	166		
24		10	367	42	57365		18052	449	1041	166		

Appendix B- Raw Data

B.4) Imaging Session 4

Table B.4a) Raw Data for 4th Imaging Session. Total raw counts per background, whole body, organ and number of cells per each area for 4th imaging session.

time	Mouse Scint 4	Image time (min)	BKG Total	#cells BKG	WB Total	#cells WB	Liver Total	#cells Liver	Lungs Total	#cells Lungs	Tumor Total	#cells Tumor
0	S4M1JI	2	2294	25	533966	2226	165537	176	76043	75		
2		5	3943	25	1012095	2226	458494	176	76188	75		
4		5	2921	25	782230	2226	386689	176	38071	75		
8		5	2319	25	497357	2226	252553	176	25723	75		
24		30	1482	25	430177	2226	215558	176	14683	75		
0	S4M2	2	167	16	331143	1861	1405	197	2803	76	1192	99
2		5	687	16	618892		66988	197	20156	76	9821	99
4		5	513	16	477617		86514	197	7148	76	14954	99
8		5	422	16			57034		3910	76	10521	99
24		30	351	16			59969		3059	76	8942	99
0	S4M3	2	160	31	318535	1987	3359	265	460	59		
2		5	1474	31			80579	265	17366	59		
4		5	511	17			78756	265	5978	59		
8		5	409	17			54335	265	3286	59		
24		30	546	17			50466	265	3806	59		

Appendix C - Calculations

AC.1 Calculations for Percent Injected Dose Gamma Camera and Error Propagation (Using Raw Data from Appendix B)

(a) Injected Dose Organ

$$ID_{(T)} = \frac{OrganNetcpm_{(T)}}{WholeBodyNetcpm_{(T=0)}}$$

$$OrganNetcpm_{(T)} = \left(\frac{TotalCountsOrgan}{\#CellsOrgan} - \frac{TotalCountsbkg}{\#CellsBkg}\right) \times \frac{1}{\text{Im}\,ageAcquistitionTime(\text{min})} \times (NumberCellsOrgan)$$

$$WBNetCPM_{(T=0)} = \left(\frac{TotalCountsWB}{\#CellsWB} - \frac{TotalCountsBkg}{\#CellsBkg}\right) \times \frac{1}{\text{Im}\,ageAcquisitionTime(\text{min})} \times (NumberCellsWB)$$

Decay Corrected Percent Injected Dose Organ

$$\%ID_{(T=0)} = (ID_{(T)})e^{0.693(T)/6.01}(100\%)$$

(B) Error Propogation

Error was propagated using a Taylor expansion formula customized by the OSU statistics department (Bill Gaeuman, Research Assistant, OSU Statistics).

The equation for biodistribution was expanded about the mean of each of its variables. The respective number of cells in each region is assumed to be constant. Variance was then equal to the square root of the sums of the squares of the partial derivatives of each term squared. The final result is as follows:

For $ID = a(N_1 - N_2)/b(N_3 - N_2)$,

$$\sigma_{ID} = sqrt\,[\,N_1(N_2 - bN_3)^2 + N_2(N_1 - aN_3)^2 + N_3(bN_1 - aN_2)^2\,]\,/\,(N_2 - bN_3)^2$$

where:

N_1 = total organ count
N_2 = total body count
N_3 = total background count
a = # cells organ / # cells background
b = # cells body / # cells background

Appendix C - Calculations

AC.2 Calculations for Injected Dose Gamma Counter (24 hr) and Error Propagation (Using Raw Data from Appendix B)

(a) Data

	S3M2	S3Control
Image Time (T=0)	12:16 pm 06/14/2005	1:20 06/14/2005
Count Time	7:40 pm 06/16/2005	7:40 pm 06/16/2005
WB Counts (Bkg Sub)$_{(T=0)}$ Camera	155859	188601
Time(hr) to Count time	57.5	56.5

Standard Data: 50 µCi in 1 ml at 10:00 am on 06/14/2005 decayed to 7:40 pm 06/16/2005 = 0.064 µCi
Standard Counts: 99027.9/min
Standard deviation for standard: ± 10% per pharmacy insert, Oregon Central Pharmacy, Eugene
Gamma Camera Efficiency (App. C): 8.5E-5 ± 2.77 E-7
Digital OHaus model SP202 scale σ = 0.01

(b) Gamma Counter Efficiency

$$Eff_{(Counter)} = \left({}^{cpm\ standard}/_{dpm\ standard} \right) = \left({}^{99027.9cpm}/_{(0.064uCi)\times(2.22E6dpm/uCi)} \right) = 0.697$$

c) Percent Injected Dose

Note: The whole body dpm was calculated from the gamma camera T=0 images for each mouse and gamma camera efficiency, previously calculated.

$$NetDPMOrgan_{counttime} = \frac{\left(\frac{CPMOrgan - CPMBkg}{WeightSample(g)} \right) * (WeightOrgan(g))}{0.697}$$

$$NetDPMWB = \left(\frac{CPMWB_{(T=0)} - BkgWB_{T=0}}{8.5E-5} \right) * e^{\frac{-0.693(HourToCountTime)}{6.01}}$$

$$24\,hour\ \%ID_{counter} = \frac{NetdpmOrgan_{(T=counttime)}}{NetdpmWB_{(decayedtocounttime)}}(100\%)$$

Appendix C – Calculations

d) Error Propagation (Gamma Counter Method)

i. Error propagation for gamma counter efficiency

$$\sigma_{gammacounterefficiency} = \sqrt{(\frac{\sigma_{stdcounts}}{stdcounts})^2 + (\frac{\sigma_{stddpm}}{stddpm})^2 + (0.1)^2}\ x\ eff = \sqrt{(314.7/99027)^2 + (376.9/142080)^2}\, x\ 0.697$$

$$= 0.07$$

where

$$\sigma_{stdcounts} = \sqrt{stdcounts} = \sqrt{99027.9} = 314.7$$

and

$$\sigma_{stddpm} = \sqrt{(sourcedpm)} = \sqrt{142080} = 376.9$$

ii. Error Propagation Gamma Camera efficiency

$$\sigma_{gammacamera} = \sqrt{(\frac{\sigma_{stdcounts}}{stdcounts})^2 + (\frac{\sigma_{stddpm}}{stddpm})^2 + (0.1)^2}\ x\ eff$$

$$= \sqrt{(\frac{399}{153583})^2 + (\frac{4.4E4}{1.81E9})^2}\ x\ 8.5\ E-5 = 2.7\ E-7$$

where,

$$\sigma_{stdcounts} = \sqrt{stdcounts} = \sqrt{153583} = 399.0$$

and

$$\sigma_{stddpm} = \sqrt{stddpm} = \sqrt{1.81E9} = 4.3E4$$

Appendix C – Calculations

Error Propagation (Gamma Counter Method) continued

iii. Error propagation Gamma Counter Biodistribution

$$\sigma_{ID} = \sqrt{\left(\frac{\sigma_{organcpm}}{organcpm}\right)^2 + \left(\frac{\sigma_{WB\ cpm}}{WBcpm}\right)^2 + \left(\frac{\sigma_{organwt}}{organwt}\right)^2 + \left(\frac{\sigma_{samplewt}}{samplewt}\right)^2 + \left(\frac{\sigma_{countereff}}{countereff}\right)^2 + \left(\frac{\sigma_{cameff}}{cameraeff}\right)^2}$$

AC.3) Weighted Averages

Weighted averages for gamma camera biodistribution were calculated according to Wang et al., 1975, pg 301. Weighted averages and their error were calculated using previously determined %ID and error values (section 4.3- Imaging Biodistribution Results) as follows:

$$weighted\ avg = \sum_{i=1}^{N}\left(\frac{x_i}{\sigma_i^2}\right) \Big/ \sum_{i=1}^{N}\frac{1}{\sigma_i^2}$$

And,

$$\sigma_{weightedAvg} = \sqrt{\frac{1}{\sum_{i=1}^{N} 1/\sigma^2}}$$

Appendix D-Calibration and Efficiency of Gamma Camera

D.1 Materials and Methods

The IS2 gamma camera was calibrated to manufacturer specifications for photopeak, energy and spatial resolution, and flood field uniformity following manufacturer's procedures. The entire calibration procedure was performed with the collimator removed from the surface of the crystal. Calibration tables are used by the IS2 acquisition software to correct for flood field uniformities after acquisition of each image is completed. Manufacturer recommends complete recalibration every three months and uniformity tables monthly. National Electrical Manufacturer's Association (NEMA) flood uniformity calculations were performed prior to each mouse imaging session to assure flood field uniformity. The camera photopeak for ^{99m}Tc was determined prior to each imaging session.

D.1.2 Photo Peaking

A 300 μCi point source of ^{67}Ga was placed at 3 meters from the face of the crystal and, using a preset acquisition which collected 40 million counts, the best fit on a linear scale was determined for the three most common energy peaks of ^{67}Ga at 93, 180 and 300 keV by the acquisition software. Once this calibration was performed, all other isotopes were peaked by intrinsic software that referenced the gallium peaks to fit the peak of the isotope in use. For ^{99m}Tc the peak was allowed to range +/- 4 keV from the actual photopeak of 141 keV before recalibration of the system was required

D.1.3 Energy Resolution

Energy tables were acquired using preset software included in the IS2 calibration software. For ^{99m}Tc a 300 to 500 μCi point source was placed approximately 3 meters from the face of the crystal. Count rate was not allowed to exceed 21,000 cps. 200 million counts were acquired and energy tables were determined for each acquisition matrix size possible

(64x64x16, 128x128x16, 512x512x16, and 1024x1024x16 pixels). This process took approximately 5 hours to complete.

D.1.4 Flood Field Uniformity

Uniformity tables were acquired using the IS2 calibration software. A 200 million count flood was acquired using a ^{99m}Tc point source of approximately 300 to 500 μCi placed at 3 meters from the face of the crystal. Count rate was not allowed to exceed 21,000 cps. Uniformity for each acquisition size was determined.

D.2 Gamma Camera Efficiency

D.2.1 Materials and Methods

Gamma Camera imaging efficiency for ^{99m}Tc activity in a mouse model was determined to obtain an alternative method for determination of injected dose.

A "mouse phantom" was fashioned using a 35 ml syringe with 25 ml solution containing a NIST traceable 1.047 mCi ^{99m}Tc source in water and normal saline. Average weight for C57blk-J6 mice is approximately 25g and tissue weight approximates H_20 at 1.0 g/ml. 9 images in a random pattern which included the entirety of the gamma camera useful field of view, were acquired for 1 minute each using a 512 x 512 x 16 pixel matrix. (Figure D.2a) The mouse phantom was approximately 5 cm from the collimator for all acquisitions. Activity of the NIST traceable ^{99m}Tc source was decay corrected to each image time and efficiency for each one of nine regions was calculated.

Appendix D-Calibration and Efficiency of Gamma Camera

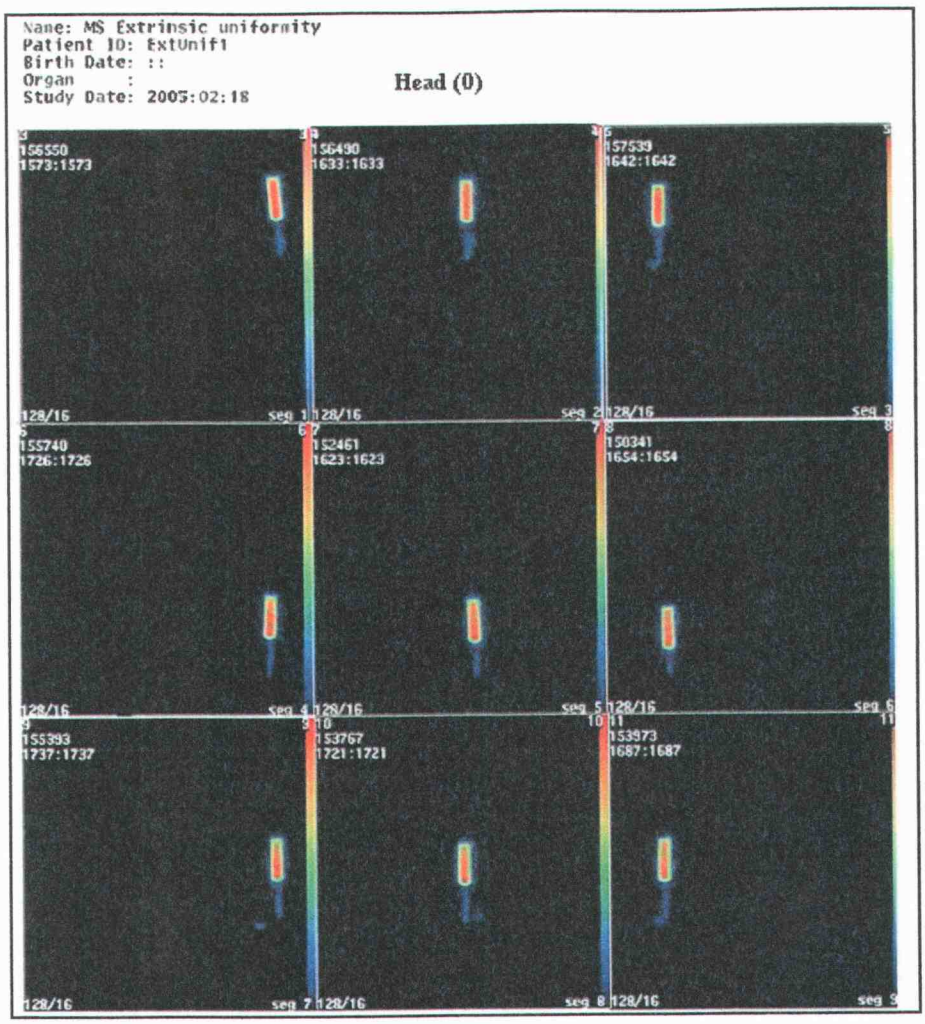

Figure D.2a)Gamma Camera Efficiency. Images of mouse models fashioned from 25 ml syringe containing 1 mCi ^{99m}Tc and placed randomly over face of gamma camera.

The following equation was used to decay correct the NIST traceable source to image time for each segment:

$$CPM_0 = CPMe^{\lambda T}$$

where,

λ = decay constant for ^{99m}Tc = 0.693/6.01 = 0.115 hr^{-1}

T = time between calibration and image

Appendix D
Calibration and Efficiency of Gamma Camera

Efficiency for each partition was then determined as follows:

$$Efficiency = \frac{CPM\ image_{t=0}}{\left(Activity\ source_{t=0}\ (uCi)\right) \times \left(2.22E6\ dpm/uCi\right)}$$

The results were averaged to determine overall gamma camera efficiency.

D.2.2 Gamma Camera Results

The gamma camera efficiency over the entire face of the collimated detector for the ^{99m}Tc mouse model was 8.5E-5 with a standard deviation of +/- 1.7E-6. Data for this determination are shown in table A.2b and A2c. All data points except one were within 2 SD of the average value. The outlier was within 3 SD of the average. The Chi Square goodness of fit test for the data showed χ^2 = 2.6E-7 < 15.5 for 8 degrees of freedom at 95% confidence (0.05).

Table D.2b) Gamma Camera Efficiency. Raw data and decayed activity for calculation of gamma camera efficiencies using a mouse model

Mouse Model Efficiencies for Gamma Camera					
1047 uCi 99mTc calibrated for 2:00.					
Segment	Time	cpm/image	Time Difference (T)	Decayed Activity (uCi)	Decayed dpm
1	4:09 PM	156550	2.09	822.7816589	1826575283
2	4:11 PM	156490	2.11	820.8863819	1822367768
3	4:13 PM	147539	2.13	818.9954708	1818169945
4	4:16 PM	155740	2.16	816.1672678	1811891335
5	4:17 PM	152461	2.17	815.2267055	1809803286
6	4:18 PM	150341	2.18	814.2872271	1807717644
7	4:19 PM	155393	2.19	813.3488314	1805634406
8	4:21 PM	153767	2.21	811.4752829	1801475128
9	4:22 PM	153973	2.22	810.5401277	1799399084

Appendix D - Calibration and Efficiency of Gamma Camera

Table D.2c) Calculated Efficiency, SD and Chi Sq for gamma camera..

		χ2 critical = 15.59 @ 95% confidence
Segment	Efficiency	Chi Statistic
1	8.57068E-05	9.69768E-09
2	8.58718E-05	1.35466E-08
3	8.1147E-05	1.57365E-07
4	8.59544E-05	1.57146E-08
5	8.42418E-05	3.67501E-09
6	8.31662E-05	3.14778E-08
7	8.60601E-05	1.87234E-08
8	8.53562E-05	3.64758E-09
9	8.55691E-05	6.97581E-09
Avg	8.47859E-05	
SD	1.66268E-06	
2SD	3.32536E-06	
3SD	4.98804E-06	
χ2		2.60824E-07

D.2.3 Conclusion

Over all, the IS2 gamma camera worked well for this experiment. A full tune including peaking with ^{67}Ga, energy tables and uniformity tables was performed prior to each mouse imaging session in order to ensure the best uniformity and resolution of images.

The gamma camera efficiency for a ^{99m}Tc mouse model was 8.5 E-5 with SD +/- 1.7E-6. The Chi Square goodness of fit test for the data showed χ^2 = 2.6E-7 for 8 degrees of freedom at 95% confidence (0.05). The mouse model efficiencies for the gamma camera were calculated to determine T=0 WB activity for biodistribution calculation.

Appendix E - Calibration of Dose Calibrator

E.1 Materials and Methods

Accuracy, geometric dependence and linearity were determined for the Victoreen Cal/Rad Isotope Calibrator in nuclear medicine prior to labeling experiments to ensure accuracy of measurements under differing conditions. Syringes containing ^{99m}Tc pertechnetate were assayed using a NIST calibrated dose calibrator at Oregon Central Pharmacy. All other sources used were certified NIST traceable reference standards. Calibration was carried out according to the procedures specified in NRC Regulatory Guide 10.8 Appendix C.

E.1.1 Accuracy

Accuracy was determined using NIST calibrated ^{137}Cs and ^{57}Co on the ^{99m}Tc dial setting of the Victoreen dose calibrator. The activity of each source was assayed on the ^{99m}Tc setting of the NIST calibrated dose calibrator at Oregon Central Pharmacy the same day. Certified activity for the ^{137}Cs and ^{57}Co reference sources was 14.282 MBq (0.386 mCi) and 45.51 MBq (1.23 mCi), respectively. Three readings for each isotope were recorded and variance between readings determined.

E.1.2 Geometric Dependence

Geometric dependence was determined using a 3 ml syringe containing 555 MBq (15 mCi) at volumes ranging from 0.5 to 2.5 ml and a 5 ml syringe containing 925 MBq (25 mCi) at volumes ranging from 0.5 to 4.0 ml of ^{99m}Tc pertechnetate. Each container was assayed on the Victoreen Cal/Rad dose calibrator set on the ^{99m}Tc dial setting. The 1.0 ml volume was selected as the standard volume against which all other assay variances were calculated.

E.1.3 Linearity

A linearity check was performed using an initial calibrated source of 6984.5 MBq (188.77 mCi). Readings were taken at timed

intervals over 2 days and the results were plotted on semi-log graph paper for activity versus time. A best-fit line was drawn through the data points and deviation for the farthest point from the line was determined using the following equation:

$$\frac{inv\ Log\ observed\ activity - inv\ Log\ trend\ line\ activity}{inv\ Log\ trend\ line\ activity}$$

E.1.4 Correction Factor for Accuracy

Using NIST traceable sources, a correction factor for accuracy of the well detector was determined. Activity was assayed using a 1.035 mCi ^{99m}Tc source in 500 µl in a 1 ml syringe and a 50.0 mCi ^{99m}Tc source in 500 µl in a 3 ml syringe. Each source activity was read a total of 21 times and the sources were repositioned in the well prior to each reading. Expected readings were decay corrected from the initial calibrated activity time point to each assay time point. A correction factor was determined using the average of the variances of the readings from the expected activity for each source.

E.2 Results

E.2.1 Accuracy

For dose calibrator accuracy, variance between readings and the certified activity of the reference source should not vary by more than +/ 5%. Results of the accuracy tests are shown in Table E.2a and indicate accuracy of the Victoreen Cal/Rad was not within tolerance specified in Reg Guide 10.8.

Appendix E - Calibration of Dose Calibrator

Table E.2a) Dose Calibrator Accuracy Check

Isotope	True Activity (mCi)	Reading (mCi)	Variance from True (%)
^{137}Cs	0.386	0.260	-32.6
		0.290	-24.9
		0.310	-19.7
^{57}Co	1.23	0.870	-29.3
		0.900	-26.8
		0.840	-31.7

E.2.2 Geometric Dependence

Dose calibrator for geometric accuracy should not vary from the selected standard activity by more than +/- 5%. Results of the geometry test (Table A.2b) showed the variance of all readings from the selected standard geometry volume of 1 ml was within +/- 5% for all geometries.

Table E.2b) Geometry Data for Victoreen Dose Calibrator

Container Geometry and Activity	Volume (ml)	Reading (mCi)	Variance (%)
2 ml syringe – 15 mCi (555 MBq)	0.5	15.19	-0.03
	1.0	15.40	0.00
	1.5	15.52	-0.01
	2.0	14.90	0.03
	2.5	14.88	0.03
3 ml syringe – 25 mCi (925 MBq)	0.5	25.43	0.02
	1.0	25.90	0.00
	2.0	26.26	-0.01
	3.0	25.77	0.01
	4.0	24.78	-0.04

Appendix E - Calibration of Dose Calibrator

E.2.3 Linearity

Data are shown in Table E.2.3a and results of the linearity test are shown in Figure E.2.3b. Deviation from the "best-fit" line should be no more than ±0.05, however, the Victoreen linearity test showed a deviation of 0.07.

Table E.2.3a) Data for Victoreen Cal/Rad Dose Calibrator *linearity determination*

Date	Time	Elapsed Time (hr)	R1 (mci)	R2 (mCi)	R3 (mCi)	R Avg (mCi)	Log R Avg	Expected Reading
Day 1	12:30	0	206.00	207.80	210.20	208.00	2.32	188.77
	5:00	4.5	124.80	124.40	121.70	123.63	2.09	112.26
Day 2	8:15	19.75	20.92	21.31	20.95	21.06	1.32	19.85
	12:15	23.75	13.01	13.50	13.15	13.22	1.12	12.51
	15:15	26.75	9.60	9.41	9.31	9.44	0.97	8.59
Day 3	8:30	44	1.15	1.19	1.28	1.21	0.08	1.17
	12:15	47.75	0.85	0.85	0.85	0.85	-0.07	0.76
	15:30	51.5	0.64	0.63	0.62	0.63	-0.20	0.54
Day 4	8:30	68.5	0.10	0.09	0.07	0.09	-1.06	0.08

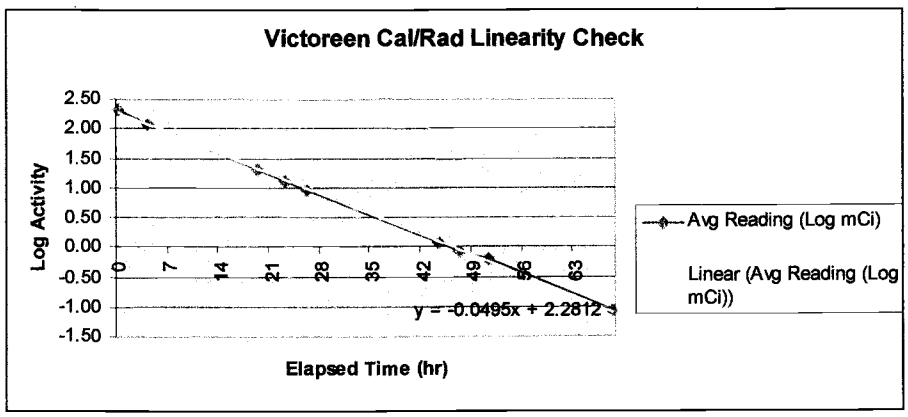

Figure E.2.3b) Linearity for Victoreen Cal/Rad. Graph of Log activity verses elapsed time shows trend line (yellow) and actual readings (red). The maximum deviation of 0.07 was at t=51.5 hours. Deviation was calculated from procedure outlined in NRC Regulatory Guide 10.8 Appendix C.

Appendix E - Calibration of Dose Calibrator

E.2.4 Correction factor for Accuracy

The correction factors for the Victoreen Cal/Rad dose calibrator were 1.125 +/- 1.57% for the 1.035 mCi source and 1.126 +/- 0.2% for the 50 mCi source at 95% confidence level for each. The correction factor was applied as 1.1255 for all readings. Data are shown in Table E.2.4a. and Table E.2.4b

E.3 Conclusion

The Victoreen dose calibrator was used for radioactivity assay of dose prior to injection and quality assurance of the labeled peptide. Therefore, it was necessary to ensure the detector was working properly.

The Victoreen Rad/Cal dose calibrator was the only feasible well detector available for radioactivity assay during this experiment. Linearity fell outside the NRC recommendation of 5% variation at approximately the 0.5 mCi activity. Since the calibration requirements do not extend to radioactive doses administered to animals, we felt that the small deviation from the NRC recommended linearity for this dose calibrator would not interfere significantly with our results.

Accuracy was not within tolerance of ± 5% for either the ^{137}Cs or ^{57}Co NIST traceable sources (Reg Guide 10.8 Appendix C). Readings for these sources were approximately 20-30% lower than expected while the NIST traceable ^{99m}Tc sources read 7-25% lower than expected. A correction factor was determined to use with the dose calibrator ^{99m}Tc setting since it was the only viable detector available for laboratory use. Ultimately, it was not required that actual injected dose be assayed on this instrument since the alternative gamma camera method was available. It was however, necessary to determine percent labeled peptide and syringe activity prior to injection with the dose calibrator. Therefore, even with the use of a correction factor for ^{99m}Tc, it is not possible to say that percent labeled peptide as reported is accurate. In addition, while the dose calibrator got us close to the desired injection activity, there was probably some variation in

uniformity for assayed activity from one syringe to the next. This was not significant since the gamma camera was ultimately used to determine injected dose.

Appendix E - Calibration of Dose Calibrator

Table E.2.4a) Data for accuracy correction factor of Cal/Rad Dose Calibrator using 1 mCi ^{99m}Tc NIST traceable source. All calculations were made using Microsoft Excel® spreadsheet.

Nuclear Med Dose Calibrator				
Accuracy Determination 1.035 mCi ^{99m}Tc calibrated for 0930 (0.5 uL in 1 cc syringe)				
Reading	Time (min post calibration)	Observed Activity(mCi)	True Activity(mCi)	True-Observed/True
1	35	0.90	0.967564129	0.07
2	36	0.79	0.965703359	0.18
3	37	0.80	0.963846169	0.17
4	38	0.88	0.961992549	0.09
5	39	0.85	0.960142495	0.11
6	40	0.81	0.958295998	0.15
7	41	0.81	0.956453053	0.15
8	42	0.87	0.954613652	0.09
9	43	0.84	0.952777788	0.12
10	44	0.82	0.950945455	0.14
11	45	0.77	0.949116646	0.19
12	46	0.77	0.947291354	0.19
13	47	0.92	0.945469572	0.03
14	48	0.86	0.943651294	0.09
15	49	0.84	0.941836512	0.11
16	50	0.71	0.940025221	0.24
17	51	0.92	0.938217413	0.02
18	52	0.81	0.936413082	0.13
19	53	0.80	0.93461222	0.14
20	54	0.86	0.932814822	0.08
21	55	0.81	0.931020881	0.13
			Avg Deviation	0.12500304
			SD	0.04305371
			95% CI	0.0156664
			Correction Factor (multiply reading by)	**1.12500304**

Appendix E - Calibration of Dose Calibrator

Table E.2.4b) Data for accuracy correction factor of Cal/Rad Dose Calibrator using 50 mCi ^{99m}Tc NIST traceable source. All calculations were made using Microsoft Excel® spreadsheet

Nuclear Medicine Dose Calibrator				
50 mCi ^{99m}Tc calib for 1000				
Reading	Time (min post calibration)	Observed Activity	True Activity	True-Observed/True
1	27	43	47.46763002	0.09411951
2	27	40.1	47.46763002	0.15521377
3	28	41.8	47.37634272	0.11770311
4	28	41.9	47.37634272	0.11559235
5	29	40.84	47.28523099	0.13630537
6	29	40.7	47.28523099	0.13926613
7	29	43.6	47.28523099	0.0779362
8	29	42.8	47.28523099	0.0948548
9	30	42.1	47.19429447	0.10794302
10	30	41.3	47.19429447	0.12489422
11	30	41.9	47.19429447	0.11218082
12	30	40.71	47.19429447	0.13739573
13	31	41.1	47.10353284	0.12745398
14	31	40.9	47.10353284	0.13169995
15	31	42.1	47.10353284	0.10622415
16	31	41	47.10353284	0.12957697
17	33	39.74	46.92253289	0.15307215
18	33	40.2	46.92253289	0.14326876
19	33	40.12	46.92253289	0.14497369
20	34	39.79	46.83229389	0.1503726
21	34	39.5	46.83229389	0.15656491
			Avg. Deviation	0.12650534
			SD	0.01781904
			95% CI	0.00024357
			Correction factor (multiply by)	**1.12650534**

Appendix F - Dose Estimation to Extremities for Imaging

F.1 Materials and Methods

Dose reconstruction for the imaging portion of the study was performed using MicroShield version 5.5 (5.05-00615). The modeled source was a simple cylinder in the dimensions of a typical mouse (height 7.62 cm, radius 1.9 cm) with 1 mCi ^{99m}Tc uniformly distributed throughout. Calculation point was the middle of the cylinder at 1 cm from the mouse. Shielding material was 1.9 cm tissue (density 1.04 g/cm^3) and 1 cm air (1.22 E-3 g/cm^3). (Figure A.4.1-1). Holding time for each mouse was assumed to be 10 minutes for anesthesia and imaging and, therefore, 6 mice could be imaged per hour. The initial dose rate determined by MicroShield was decayed for each imaging time point, multiplied by a time factor, then added to determine total estimated dose to the extremities for imaging. The badges and finger rings employed were sent for analysis immediately following the first procedure to assess actual dose acquired for one imaging session.

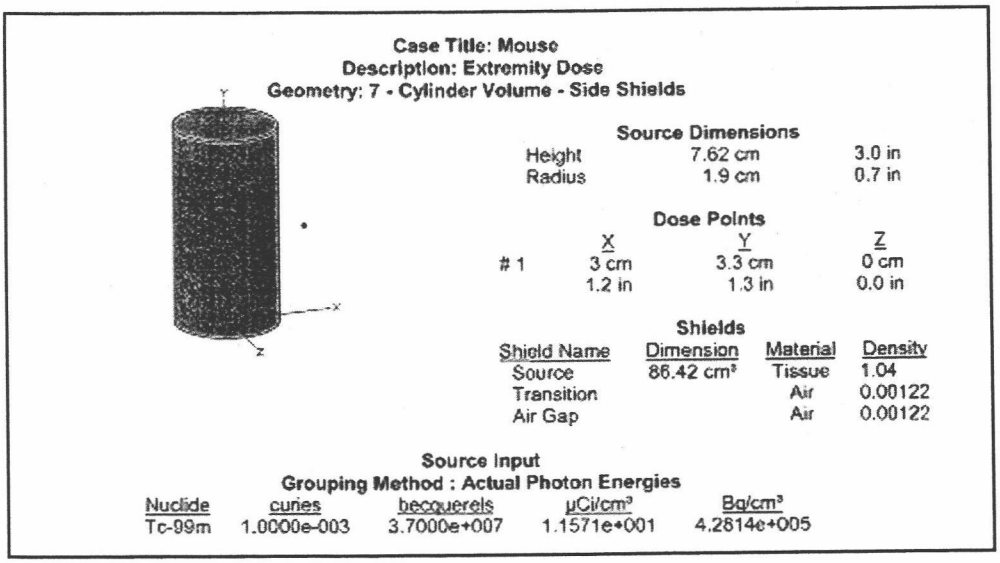

Figure F.1a) Input parameters for MicroShield code calculation of dose rate to the extremities for 1 mCi ^{99m}Tc distributed uniformly in a mouse.

Appendix F - Dose Estimation to Extremities for Imaging

F.2 Results

The MicroShield calculated dose rate for 1 mCi ^{99m}Tc in a mouse was 68.5 mR/hr. The total dose for an imaging session was 275.5 mR if each mouse was held a total of ten minutes per time point. The total dose for an imaging session was 138.0 mR if each mouse was held a total of 5 minutes for each time point. (Table F.2a)

Table F.2a) Calculated total dose to extremities per imaging session.

Image Time Point (hr)	**Dose Rate (mR/hr)**	**Dose Estimate (mR) (6 mice 10 min each)**	**Dose Estimate (6 mice 5 min each)**
T=0	68.5	68.5	34.3
T=1	61.0	61.0	30.6
T=2	54.4	54.4	27.2
T=4	43.2	43.2	21.6
T=8	27.2	27.2	13.6
T=12	17.1	17.1	8.6
T=24	4.3	4.3	2.1
Total		**275.5**	**138.0**

The actual dose received to the extremities as determined by offsite analysis of the finger rings was 296 mrem. When the correction factor of 0.93 mR/mrem is applied to the MicroShield estimation for a holding time of 10 minutes, the estimated dose to the extremities in mrem is 296 mrem. This agrees nicely with the data for a holding time of 10 minutes per mouse per imaging time point.

F.3 Conclusion

The calculated estimated dose to extremities agrees nicely with the actual dose to extremities when the mice are held for 10 minutes each per imaging time point.